MOTION PLANNING AND CONSTRAINT EXPLORATION FOR ROBOTIC SURGERY

By

Sam Bhattacharyya

Thesis

Submitted to the Faculty of the

Graduate School of Vanderbilt University

in partial fulfillment of the requirements

for the degree of

MASTER OF SCIENCE

In

Mechanical Engineering

December 2011

Nashville, Tennessee

Approved:

Professor Nabil Simaan

Professor Nilanjan Sarkar

ACKNOWLEDGEMENTS

This work would not have been possible without the financial support of the NSF, and the Vanderbilt Department of Mechanical Engineering. I would also like to thank my lab-mates, classmates, the department staff, my professors, my thesis committee, 5 hour energy™ and of course my advisor Professor Nabil Simaan. $G(tb)^2$.

TABLE OF CONTENTS

Page

NOMENCLATURE

Table 1: A list of symbols and nomenclature used in this publication

Symbol	Description
$\boldsymbol{\zeta}$	7 Dimensional gripper position/orientation in space
$\boldsymbol{r}$	3-dimensional Cartesian position
$\widehat{\boldsymbol{q}}$	4-dimensional quaternion orientation
$\boldsymbol{\xi}$	6 – dimensional twist vector in Cartesian space
$\boldsymbol{w_e}$	Elastic reaction Wrench, exerted on the environment by the gripper
$\boldsymbol{K}$	Local Stiffness Matrix
E	Elastic energy exerted on the elastic system by the gripper
C	Designation for Mechanical Constraint
C_v	Constraint Vector
J	Path Planner Optimization function
$\boldsymbol{\Gamma}$	Diagonal Dimensional weighting matrix
Ξ	Designation for Stiffness Region
Δ	Axis coordinate conversion matrix
h	Screw pitch
λ	Eigenvalue
μ	Principle Rotational Stiffness
σ	Principle Translational Stiffness
α	Dimensional weighting factor

LIST OF FIGURES

LIST OF TABLES

CHAPTER I

I INTRODUCTION

I.A Motivation

Commercial surgical assistance systems, such as the Intuitive Surgical ™Da-Vinci robotic system [1], continue to gain adoption in hospitals around the country, due to their ability to augment surgeons' skills (e.g. dexterity and accuracy). Though significant progress has been made by existing commercial systems, they are almost exclusively teleoperated (i.e. they are *passive* manipulators); thus, they ultimately place the entire burden of safeguarding the anatomy on the surgeon. As the next generation of robotic surgical assistants (RSA) are developed, the functionality and complexity of emerging systems such as [2], [3], [4] calls for the development of *intelligent* surgical robotic slaves that continuously gather information about their environment and actively participate in aiding the surgeon in completion of surgical subtasks. This vision of intelligent, semi-autonomous RSAs, which can coordinate with surgeons in performing menial tasks, will allow surgeons to focus on more crucial aspects of the operation, while seamlessly manipulating high DoF robots, and safeguarding the anatomy against trauma.

An example of an application scenario is the manipulation of a kidney, by several robotic arms, during a nephrectomy procedure. An intelligent slave, which can determine the mechanical properties of the suspended organ in its current configuration, can then coordinate the motion of all arms to safely manipulate the suspended organ, while

allowing the surgeon to command movement of one arm or specify target retraction distance from the surgical site. Another application would the manipulation of organs within the abdominal cavity, in order to gain access to underlying tissues. A cooperative intelligent RSA would be able to determine the mechanical properties of the obstructive organ, and automatically move it in order to increase visibility of/open up access to the critical underlying tissue.

This aim of this work is three fold: To propose a framework for modeling and characterizing the mechanical properties of an unknown elastic system, to propose algorithms for safe autonomous manipulation of tissues in an unknown environment and finally to propose a methodology for detecting and identifying mechanical constraints of an arbitrary unknown elastic system. Used in tandem, these tools can enable an intelligent RSA to autonomously perform surgical subtasks without a priori knowledge of the workspace, while simultaneously mapping the elastic properties of the environment.

I.B Problem Statement and Scope

For the purposes of this work, we consider a standard 6 degree of freedom (DoF) manipulator, with an attached robotic gripper, operating in an unknown and flexible environment. The robot operates in a full 6-dimensional Cartesian workspace, and is grabbing some semi-rigid object, which is suspended within an elastic environment, as shown in the figure below. Our definition of semi-rigid is such that, though the object internal deformation of the object is noticeable smaller than its elastic connections to the environment. Actual magnitudes will vary with the application, and the environment.

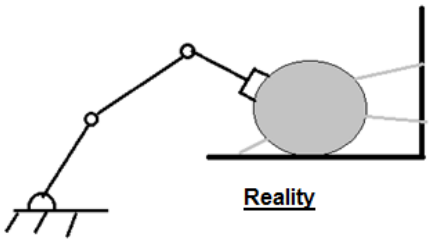

Figure 1: Semi-rigid object suspended in a flexible environment

The environment is unknown, but it assumed to be stable, meaning that while surfaces may be deformable, any deformations will return back to equilibrium in the absence of disturbances.

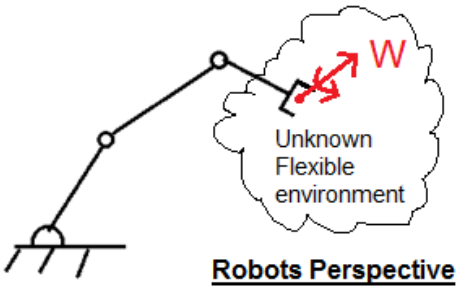

Figure 2: Unknown Environment

We represent the gripper's pose in space as $\boldsymbol{\zeta} = [\boldsymbol{r}^T, \hat{\boldsymbol{q}}^T]$, a 7 dimensional vector including its 3-dimensional Cartesian position $\boldsymbol{r} = [x, y, z]^T$, and it's 4-dimensional orientation in quaternion space $\hat{\boldsymbol{q}} = \left[q_o, q_i, q_j, q_k\right]^T$. The robot is assumed to be perfectly kinematically controllable, such that it can move in full 6-dimensional Cartesian space along any given twist $\boldsymbol{\xi} = [\boldsymbol{v_o}, \boldsymbol{\omega_o}]$ from any pose $\boldsymbol{\zeta}$ to any other pose $\boldsymbol{\zeta}'$. Furthermore,

the robot is equipped with 6-axis force sensing capability, and can measure the elastic wrench $\boldsymbol{w}_e$ acting on the robot by the environment. In this work, we are not considering any forces due to gravity, dynamics or friction, as the former two can easily be compensated for in practice, while the latter is kept out of the scope of this work, since models of internal organ friction are not available yet. .

The problem to be solved, therefore, can be stated as such: Given the initial object pose $\boldsymbol{\zeta}_i$, manipulate the object to a new pose $\boldsymbol{\zeta}_g$, while avoiding exceeding a critical force $\boldsymbol{w}_{cr}$ at any point, on the unknown elastic system, and while minimizing the elastic energy exerted on the elastic system.

This Thesis will present a solution to the aforementioned problem, and also answer the following 5 problems: 1) Develop a model to describe the elastic properties of the environment, 2) use $\boldsymbol{\zeta}, \boldsymbol{w}_e$to identify the mechanical constraints of the system, 3) Use information to intelligently navigate the workspace, 4) Create a map of these constraints throughout the workspace and 5) Use the information to aid in future manipulation tasks and goals. These problems will be sequentially solved in chapter IV and V of this thesis.

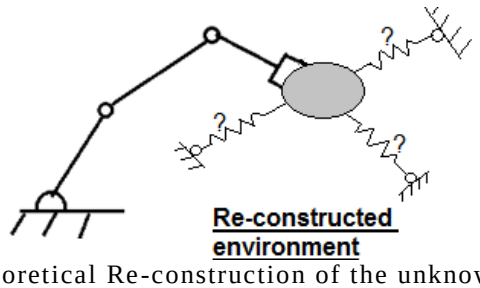

Figure 3: Theoretical Re-construction of the unknown environment

In order to develop a proper solution, a very basic assumption is made about the elastic system. Firstly, a maximum safe elastic energy/elastic force is assumed, below which exertion of such force or elastic energy will not damage the environment. The range and scales of such values will be application dependent, and while this does constitute a-priori knowledge about the environment, information of this kind of can be easily obtained through bio-mechanics references for tasks in the surgical domain.

I.C Related Laboratory Work

The work presented in this thesis was done at the ARMA lab at Vanderbilt University, under the direction of Dr. Nabil Simaan. This work ties into the work done by current and former students of the lab, who have worked in the areas of local stiffness exploration, contact and constraint detection for surgical robots. In [15], Xu and Simaan (2009) implement stiffness mapping of the surface of an organ, using the intrinsic force sensing capabilities of a snake-like RSA. In [36], [37], Goldman et al. (2010, 2011) use the same RSA for exploration of shape and local impedance of an unknown environment. Finally, in [47] Bajo et al. (2011) presented work on detection of contact for the same snake-like RSA.

I.D Contribution and outline

The primary contributions of this work are in validating the feasibility of autonomous manipulation in an unknown elastic environment, in developing a real-time

compatible representation of global stiffness properties, and in presenting methods for automatically identifying and classifying flexible constraints in real time.

Previous works on exploration mainly focus on constraint exploration in rigid environments (Lefebvre) [44], constraint identification of tools (Dupont and Howe) [9], and exploration in rigid environments (Okamura and Kutcowsky) [11]. To date, there are no clear frameworks to exploration in flexible environments. A recent exception is the work of Goldman in [36], [37] where exploration of shape, and local impedance has been carried out. This work extends these results to include the characterization of organ constraints and path planning for safe manipulation.

First, in section II, works in the related areas of path planning and environment exploration are reviewed in detail. In section III, some necessary background, including Spatial Stiffness theory and AI methods, are reviewed. An algorithm for blind, safe, autonomous manipulation is proposed in section IV, and then experimentally validated using a Puma 560 industrial robot arm. Finally, section V details our methods for characterizing, identifying and mapping the elastic constraints of a workspace in real time, and presents experimental evaluation of these techniques on real flexible objects using the Puma 560.

CHAPTER II

II LITERATURE REVIEW

There have been numerous works on the relevant topics of environmental exploration, detection of contact, constraint identification and path planning in elastic environments. The solutions presented in these works operate in restricted domains however, and only provide solutions to parts of the problem posed in the previous section.

II.A Constraint detection/identification

He [5,6] explicitly dealt with the exploration and detection of mechanical constraints ("Contact States") between two rigid objects. Xiao developed a simple model of a manipulator grasping a movable polyhedron A, which is possibly in contact with fixed polyhedron B, and represented the contact as the super-position as a combination of "principle contacts", simple dimensionless/directionless kinematic constraints. He then assumed that the geometry (shape, dimensions and position/orientation) of the objects was known, but with experimental uncertainty. Xiao simply defines a method for resolving the rigid kinematic model with the actual experimental data, to determine the most likely contact state for a given configuration of object A. This methodology works, however it requires explicit geometric information about the object being manipulated,

especially since it works entirely in the kinematic domain (constraints are not considered as reaction forces, but rather as purely kinematic constraints).

De Schutter [7] also deals with manipulation of objects with known geometries and an appropriate kinematic map (with experimental error), but tackles the problem of constraint identification, for manipulation under flexible constraints. To do this, he represents the flexible constraint of an object at a given configuration as a virtual compliant manipulator. This virtual manipulator results in the same degrees of freedom as the object, but models the compliance in each direction of motion, to provide predictions in the changes of the constraint forces as the real manipulator moves in space. This methodology allows for simple characterization/representation of elastic constraints in a given workspace, however it requires explicit kinematic models of the environment and assumes known geometries ahead of time.

Kitagaki and Suehiro [8] get rid of the assumption of known geometric/kinematic models by incorporating force information. Assuming a manipulator with an attached force sensor, manipulating an object in a rigid environment, they estimate the location of point contact using static balancing. The associated constraint results in a normal force, which will result in an applied moment on the force sensor. Furthermore, they present models for detecting edge on plane constraints, and propose methods detection of contact state transitions. This methodology is powerful and simple, however it assumes a rigid environment, and furthermore requires high accuracy force measurements of contacts with very high rigidity.

Dupont [9] presented a simple but effective method for modeling and identifying kinematic constraints of a general robotic manipulator. He does this by using the notion that, for a kinematic constraint, no constraint wrench can do any work about a freedom twist (see section III.A.2). He suggests that for a manipulator's end effector, at a certain position while moving along a trajectory, any forces/torques in the direction of the trajectory cannot be due to a constraint force, and furthermore, that any forces/torques normal to the trajectory are due to a kinematic constraint at that location. Correcting for dynamics and gravity forces at the end effector, he then utilizes this method to automatically explore the kinematic constraints on surgical instruments during insertion.

Howe [10] uses probabilistic methods to infer contact and constraint properties of a given object being manipulated, using experimental force/position data. He assumes a set of known Kinematic constraints ("Contact States"), and develops geometric models for each of these constraints, which are independent of size/scale/orientation. For a given robot manipulation task, force/kinematic data are then simultaneously evaluated on how well it matches each geometric model. A hidden Markov model is then used to stochastically determine the current contact state, using a closest fit to that contact state's model.

To the author's knowledge, none of these works deals explicitly with identification of flexible constraints in unknown environments, with the exception of course being Goldman (2011). With high-DoF RSAs further abstracting the interface between the surgeon and the patient anatomy, there is a clear need for further investigation in this area to enable proper force feedback and semi-autonomous manipulation schemes in robotic surgery.

II.B Exploration of unknown environments

Okamura and Cutkosky [11, 12] focus on the haptic exploration of objects using robot fingers which are equipped with tactile sensors. They use feature based exploration to map and characterize the surface properties of an object being grasped by a robotic hand. They define classes of features, macrofeatures, such as a 'bump' feature, or a 'ridge' feature, and present methods for detecting instances on these macrofeatures on an object being grasped. A map of these features on an object represents a tactile signature, and could then be used to identify/characterize the particular object being grasped.

Allen [13] also worked on haptic exploration of objects using robot fingers, however he focused on developing models of the geometric shape of the object, rather than mapping/characterizing the stiffness properties. Allen uses tactile and kinematic information to define a set of contact points in space, corresponding to where the fingers/hand is in contact with the object. He then fits these points to a 3-dimensional superquadric function, to recover the general form of the object in space, from a set of sparse contact data.

One alternative to representing elasticity as FEM is to use a stiffness map, map over the workspace which simply measures the magnitude of the stiffness at each location. Althoefer [14] and Xu[15] [38], both present devices which can be used to develop stiffness maps over a flexible surface, which can be used to detect specific features, such as sections of high rigidity, while exploring an elastic workspace. They do this by simple considering stiffness as the spatial derivative of force, and use the kinematic models and intrinsic force sensing capabilities of their devices to map the

stiffness in a given region. Exploration of stiffness in this manner can be used to detect features, such as tumor, on an on organ during surgery. Since such stiffness maps only explicitly consider magnitude, they cannot be used for characterizing mechanical constraints, which are inherently direction dependent at a given location. These works explore normal stiffness. Goldman extended these works to include exploration of perceived impedence tensors (damping, stiffness, inertia).

Finally, Gupta [16] presents a straightforward method for simultaneous path planning and exploration of an unknown workspace, using a robot manipulator and a tactile "skin" sensor. Using the sensor, it is assumed that contact can be measured at any point on the robot manipulator, and Gupta proposes an algorithm for systematically exploring the unknown workspace, and recording positions without contact as the "freedom space". Given sufficient time to explore the workspace, the algorithm will have developed a full map of the workspace, broken down into the "freedom space" and the constraint space.

Most of these works, which deal with contact estimation of environment exploration, assume a rigid and otherwise static environment, which, for many applications is certainly valid. Despite the progress made in environment exploration, contact detection and constraint estimation, to the best of our knowledge, little work has been done on the blind characterization and estimation of flexibly constrained objects in unknown environments.

II.C Path Planning

As opposed to environmental exploration, path planning is a subject which has had some attention, in the context of flexible/elastic environment. Using a force based approach and an FEM model, Rodriguez [17] considered the path planning issues of navigating in a completely deformable known environment. By using a Rapidly-Exploring Random Tree algorithm and a collision detection algorithm, they attempt to minimize the elastic energy in all of the possible paths that could be taken to reach the end goal. They used this path planning method to simulate a robot navigating around flexible organs/tissues within the human chest cavity.

Patil et al. [18] used finite element methods to model the elastic characteristics of a flap of tissue being manipulated during organ retraction. Patil uses an offline optimization algorithm to pre-compute an optimal path for a given manipulator to retract the tissue in order to maximize the area exposed under the flap, while minimizing the elastic energy exerted on the tissue.

Gayle et al. [19] model a deformable robot moving through a flexible environment, and proposes an algorithm which uses a finite element model and virtual dynamic equations to compute an optimal path (offline) for the robot from a start goal to a finish goal, while observing a set of hard constraints. They then apply this methodology to optimize the path for a snake robot which enters the femoral artery (in the legs) and navigates to the liver to perform some operation.

Like Rodriguez and Patil, Gayle assumed a known environment and used FEM to model its elasticity. There are many other works on path planning methods in flexible environments, but which almost exclusively deal with Finite element methods and off-line path planning. While they are effective for providing theoretically optimal paths in a given scenario, real-time implementation of these paths will never be perfect. Hence there is great potential in utilizing real time exploration of constraints.

CHAPTER III

III MATHEMATICAL BACKGROUND

III.A Stiffness, Compliance and Screw Theory

III.A.1 Screw theory

In Cartesian space, there are 6 dimensions of motion for a general rigid body: Translation along the three Cartesian axes, and rotation about each of those axes .While absolute orientation cannot be represented completely in only 3 dimensions, any Cartesian angular velocity can be expressed completely in 3 dimensions.To represent a general velocity in space, we can then define a 6 dimensional vector, which includes three translational velocities, and 3 angular velocities. This vector will be denoted as $\boldsymbol{\xi}$

$$\boldsymbol{\xi} = \begin{bmatrix} \boldsymbol{\omega_o} \\ \boldsymbol{v_o} \end{bmatrix} \tag{1}$$

Chasle's theorem forms the basis for screw theory, and can be stated as such: The most general displacement for a rigid body in space can be described as translation along a line in space, and a rotation about that same line. Plucker coordinates can be used to describe any such line in space, and are composed of 6 homogenous coordinates\

$$\begin{bmatrix} \boldsymbol{l_v} \\ \boldsymbol{r} \times \boldsymbol{l_v} \end{bmatrix} \tag{2}$$

Where $\boldsymbol{l_v}$ describes the direction of the line, and $\boldsymbol{r}$ is a vector from the origin to any point on the line. These 6 homogenous coordinates can accurately describe any line in space. Now consider again the general 6-dimensional vector $\boldsymbol{\xi} = \begin{bmatrix} \boldsymbol{\omega}_o \\ \boldsymbol{v}_o \end{bmatrix}$

The rotation around a vector (along a general line in space) can be expressed in plucker coordinates, as follows

$$\begin{bmatrix} \boldsymbol{\omega}_o \\ \boldsymbol{r} \times \boldsymbol{\omega}_o \end{bmatrix} \tag{3}$$

As can be seen, when the line is away from the origin, the rotation about that line will create a velocity normal to the line. Depending on the direction and magnitude of $\boldsymbol{r}$, any velocity normal to $\boldsymbol{l}_v$ can be expressed as $\boldsymbol{r} \times \boldsymbol{\omega}_o$. As Chasle's theorem states, any general rigid body motion can be described by the movement along a line in space, and around that line in space. Any velocity that is along the direction of the axis of rotation $\boldsymbol{l}_v$ can be modeled as a screw such that rotation around the axis is coupled with a translation along that axis, via pitch h. $\boldsymbol{v}_o \cdot \boldsymbol{l}_v = h\boldsymbol{\omega}_o$. If we add this term to the Plucker line coordinates, we get:

$$\begin{bmatrix} \boldsymbol{\omega}_o \\ \boldsymbol{r} \times \boldsymbol{\omega}_o + h\boldsymbol{\omega}_o \end{bmatrix} \tag{4}$$

Since $\boldsymbol{r}$ can be used to represent any velocity normal to $\boldsymbol{l}_v$ and h can be used to represent any velocity along $\boldsymbol{l}_v$, any general velocity can be described at $[\boldsymbol{r} \times \boldsymbol{\omega}_o + h\boldsymbol{\omega}_o]$ Thus, we can represent the general motion $\boldsymbol{\xi} = \begin{bmatrix} \boldsymbol{\omega}_o \\ \boldsymbol{v}_o \end{bmatrix}$ as a screw vector $\begin{bmatrix} \boldsymbol{\omega}_o \\ \boldsymbol{r} \times \boldsymbol{\omega}_o + h\boldsymbol{\omega}_o \end{bmatrix}$. If $h = 0$, the twist corresponds to a revolute joint. If $h \to \infty$, the twist corresponds to a pure translation.

$\boldsymbol{r}$ can be calculated as

$$\boldsymbol{r} = \frac{(\boldsymbol{\omega}_o \times \boldsymbol{v}_o)}{\left|\left|\omega\right|\right|^2} \tag{5}$$

h can be calculated as

$$h = \frac{\boldsymbol{v}_o^T \boldsymbol{\omega}_o}{\boldsymbol{\omega}_o^T \boldsymbol{\omega}_o} \tag{6}$$

Using screw theory, it is possible to analyze twist vectors to analyze centers of rotation and to classify and characterize complex rigid body motions.

It is also possible to analyze force and moments using screw theory. This is done by considering a general 6-dimensional force/moment $\boldsymbol{w}_e$

$$\boldsymbol{w}_e = \begin{bmatrix} \boldsymbol{f} \\ \boldsymbol{M} \end{bmatrix} \tag{7}$$

As done with twists, the moment can be expressed as a perpendicular component $\boldsymbol{r} \times \boldsymbol{f}$ and a parallel component $h\boldsymbol{f}$. Thus, any force/moment in space can be expressed as:

$$\boldsymbol{w}_e = \begin{bmatrix} \boldsymbol{f} \\ \boldsymbol{r} \times \boldsymbol{f} + h\boldsymbol{f} \end{bmatrix} \tag{8}$$

III.A.2 Mechanical Constraints

The concept of mechanical constraints is used to describe kinematic restrictions on the movement of rigid objects in space. Consider a general 3-dimensional rigid object suspended in 6-dimensional Cartesian space, as shown in Figure 4 below.

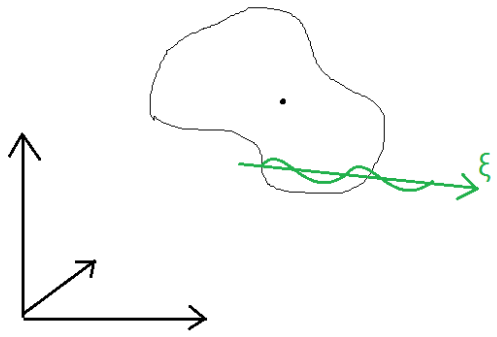

Figure 4: General rigid body motion

If there are no constraints on the movement of this object, then it can follow any general twist in 6-dimensional space (6 Degrees of Freedom), without restriction. For most practical applications in robotics/engineering, this is usually never the case, as objects aren't simply suspended in space. Rather, most objects at rest are constrained from motion along certain directions, due to gravity, friction and contact with the environment, and are thus restricted the fewer than 6 degrees of freedom. As an example, consider a book lying on a table, as shown below:

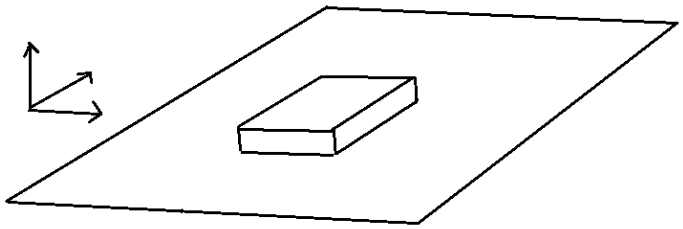

Figure 5: Planar Constraint

The book is free to slide along the table, and can rotate around the normal axis of the table. It is, however, restricted from moving into the table, and from rotation around axes in the plane of the table. Thus, it has been restricted to 3 DoF, by restrictions along 3 directions of motion. This particular form of motion restriction is known as a planar constraint, which is one of a large set of mechanical constraints. A mechanical constraint is composed of a set of restrictions on the motion of an object along a set of directions. The directions along which there is no motion restriction are known as freedom twists $\boldsymbol{\xi}$, since twists along these directions incur no resistance. Directions along which motion is impeded, due to rigid body contact or friction, are known as constraint wrenches $\boldsymbol{w}$, as reaction wrenches along these directions prevent rigid objects from moving along them.

There are a number of different general rigid body constraints, that are represented by constraint wrenches and freedom twists. A few are described below:

III.A.2.a Pin joint

One of the most common types of constraints is a pin-joint constraint, as shown in the diagram below. Pin joints contain only one DoF, rotation along an axis. Accordingly, the joint itself is composed of 5 constraint wrenches, which prevent Cartesian translation of the joint, as well as rotation around axes which are perpendicular to the primary axis of rotation.

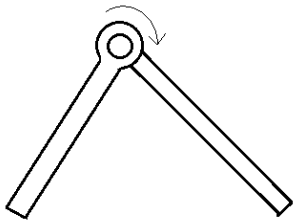

Figure 6: Pin Joint Constraint

Real examples of pin-joints would include any type of hinge, or a robotic arm.

III.A.2.b Peg-in-Hole

A less common type of constraint is a cylinder constraint, which has 2 DoF, and is modeled as a cylinder-peg inside a circular hole. The cylinder is allowed to translate back and forth along it's axes, as well as to rotate around it's own axis.

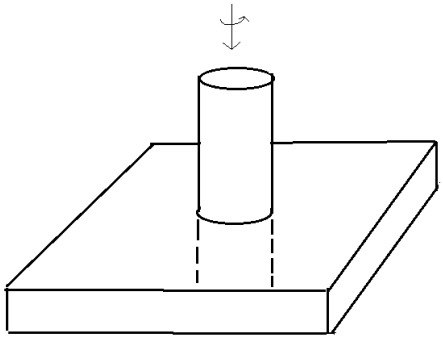

Figure 7: Peg in hole constraint

III.A.2.c Ball joint

Ball joints are very typical constraints, and allow free rotation along any axis, while restricting translation along any axis.

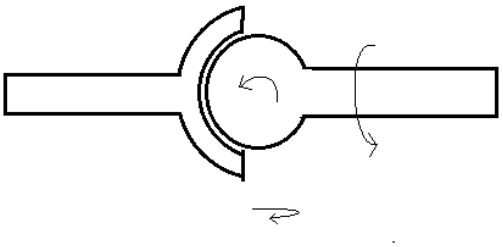

Figure 8: Ball joint constraint

Real examples of ball joints include any shoulder joints. These, along with a large set of other rigid mechanical constraints are used to describe the mechanical/kinematic properties of general rigid bodies suspended in an environment.

III.A.3 Spatial Stiffness in the context of screw theory

For surgical applications, in which we wish to describe objects suspended in unknown elastic environments, the rigid mechanical constraint models described above are no-longer applicable. Fortunately, there has been a great deal of work done in the late 90's and early 2000's to analyze spatial stiffness and elastic environments using screw theory, allowing simpler representations of complex elastic behavior and providing insight into the fundamental elastic properties of the system.

For an object suspended in an elastic environment (see figure 9), perceived constraint stiffness matrix $\boldsymbol{K}$ is defined as the linear map between an infinitesimal twist $\delta\boldsymbol{\xi}$ of the object, and the resulting change in the reaction wrench $\boldsymbol{\delta w_e}$ from an equilibrium pose.

$$\delta \boldsymbol{w_e} = \boldsymbol{K}\delta\boldsymbol{\xi} \tag{9}$$

Schimmels and Huang [20], Roberts[21,22], Lipkin [23] and others have shown that the local stiffness $\boldsymbol{K}$, can be represented as the linear combination of several springs acting in parallel, as long as $\boldsymbol{K}$ is Symmetric, positive semi-definite.

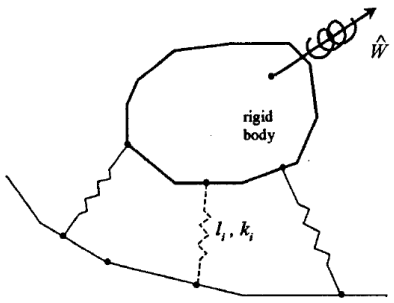

Figure 9: Spatial Stiffness model

This is done via matrix decompositions of $\boldsymbol{K}$, and provides a more intuitive representation of the stiffness than the regular stiffness matrix, as well as some information about the fundamental properties of the system.

The Eigenvalue problem of $\boldsymbol{K}$ (equation 10) is one such decomposition, and yields 6 eigenvectors and eigenvalues. The system can then be modeled by 6 complex springs (springs with both linear and torsional components), each with a direction and magnitude of one of the eigenvectors and its associated eigenvalue respectively.

$$\boldsymbol{K}\boldsymbol{e} = \lambda \boldsymbol{e} \tag{10}$$

Like many other decompositions, this one is not frame-invariant, and will result in different eigenvectors and eigenvalues, based on the frame being considered. While the eigenvectors will never be frame independent, both [32] and [33] present modified eigenvalue problems which will yield frame invariant eigenvalues.

Schimmels proposes the "Eigenscrew Decomposition", in which the only modification is a delta matrix $\Delta = \begin{bmatrix} \mathbf{0}_{3\times3} & \boldsymbol{I}_{3\times3} \\ \boldsymbol{I}_{3\times3} & \mathbf{0}_{3\times3} \end{bmatrix}$ and formulates the eigenscrew problem as in equation (11)

$$\boldsymbol{K}\Delta\boldsymbol{e} = \lambda \boldsymbol{e} \tag{11}$$

The effect of the Δ matrix is to interchange the first and last three elements of a 6-dimensional axis, which converts between axis screw coordinates ($\delta\boldsymbol{\xi} = \begin{bmatrix} \delta x \\ \delta\theta \end{bmatrix}$) to ray screw coordinates $\delta\boldsymbol{w}_e = \begin{bmatrix} \delta\boldsymbol{f} \\ \delta\boldsymbol{M} \end{bmatrix}$, in order to preserve the units. This yields a set of eigenvalues which are frame invariant, in units of N/rad, and as Schimmels argues, provides insight into the fundamental nature of the problem.

Lin [39] breaks K into sub-matrices $K_{6\times6} = \begin{bmatrix} A_{3\times3} & B_{3\times3}^T \\ B_{3\times3} & D_{3\times3} \end{bmatrix}$, uses matrix algebra to cancel out frame-dependent components of K, resulting in the following sub-matrices

$$K_v = D - B^T A^{-1} B \qquad K_w = A \tag{12}$$

Where the eigenvalues $\mu_1, \mu_2, \mu_3$of K_v are the principle rotational stiffnesses of $\boldsymbol{K}$, the eigenvalues $\sigma_1, \sigma_2, \sigma_3$ of K_w are the principle translational stiffnesses of $\boldsymbol{K}$**.** The result is a set of 3 orthogonal, rotational axes and set of 3 orthogonal translational axes, whose magnitudes are frame invariant and describe the pure rotational and pure translational behavior of the system.

Lipkin [25] uses a similar analysis to define the principle rotational stiffness axes and the principle translational compliant axes of a stiffness matrix K, and then uses them to create rotational and translational elasticity ellipsoids.

The tools outlined above can and will be used to analyze the mechanical properties of unknown elastic environments. As Schimmels et al. discuss [24], any proper eigenvalue or eigenscrew decomposition requires a Symmetric, positive, Semi-Definite (SPSD) matrix, which is almost never obtainable from experimental numbers (due to noise and displacement from equilibrium). Thus, in order to experimentally implement this analysis, an SPSD matrix needs to be derived from experimentally gathered data. Ellis and McAllister [26] present a method of doing so, by using an SPSD approximate K_{SPSD} of a given experimentally derived stiffness matrix $\boldsymbol{K}$**.** The solution is explained in [27] and is summarized below:

$$B = \frac{K + K^T}{2} \tag{13}$$

Take the Eigenvalue decomposition of B

$$BZ = \Lambda Z \tag{14}$$

Where Z is a matrix of eigenvectors and Λ is a diagonal matrix of eigenvalues.

$$H = Z|\Lambda|Z^T \tag{15}$$

$$K_{SPSD} = \frac{B + H}{2} \tag{16}$$

The result is a close approximate of the stiffness matrix K, which will not include negative or complex eigenvalues.

III.B Numerical Optimization and Stochastic Methods

The previous chapter presented an entirely analytical framework for describing and understanding flexibility and spatial stiffness using screw theory. When the necessary information is available, and the analytical models are applicable, analytical methods are effective, efficient and provide broader insight into the structure of the problem.

In real world applications such as robotic surgery however, complete information almost never available. In order for an autonomous Robotic Surgical Assistant to operate is any such environment, it has to explore, gather data, and make intelligent decisions using incomplete information, without compromising the safety of the patient. To tackle these problems, a variety of numerical, computational and AI methods can be used. This chapter will discuss the ideas of Numerical Optimization, Clustering, Markov models, Particle Filtering and Monte-Carlo methods.

III.B.1 Numerical Optimization

Consider some function $f(\boldsymbol{x})$, which is a function of many variables for which computation of $f(\boldsymbol{x}) = y$ is easy, while the inverse $f^{-1}(y) = \boldsymbol{x}$ is highly intractable.

The problem of optimization (finding the $\boldsymbol{x}$ which will minimize/maximize y) usually cannot be solved analytically, even though evaluating the function is trivial. For this situation, numerical methods can be utilized to navigate the domain space $\boldsymbol{x} \in \mathfrak{R}^{\boldsymbol{n}}$, and find the vector of inputs $\boldsymbol{x}^*$ which will locally or globally minimize $f(\boldsymbol{x})$.

III.B.1.a Steepest Descent

The simplest numerical optimization method is known as the steepest descent method. Starting from the current parameter vector $\boldsymbol{x}$, the steepest descent method evaluates the derivative $\frac{df}{d\boldsymbol{x}}$, and moves in the direction of $\frac{df}{d\boldsymbol{x}}$ in configuration space, by incrementing $\boldsymbol{x}$ by $\alpha \frac{df}{d\boldsymbol{x}}$. The algorithm is summarized below, in Figure 10.

Steepest Descent Algorithm

Given starting configuration $\boldsymbol{x} = \boldsymbol{x}_o$

While $(|\boldsymbol{x} - \boldsymbol{x}^*| < \epsilon)$

- $\boldsymbol{p} = -\frac{df}{d\boldsymbol{x}} \Big/ \left|\left|\frac{df}{dx}\right|\right|$
- $\boldsymbol{x} = \boldsymbol{x} + \alpha \boldsymbol{p}$

Figure 10: Steepest Descent Algorithm

The Steepest Descent method is a good basic numerical optimization algorithm, but suffers from slow convergence [40]. More effective gradient techniques exist [29] (Newton/Quasi-Newton), but require more information, such as the Hessian of f, $\frac{d^2 f}{dx^2}$

III.B.1.b Non-Linear Optimization

One such hessian based algorithm is the typical non-linear optimization function. For example, consider a non-linear system $(\boldsymbol{x})$, where $\boldsymbol{x}$ represents the hidden inputs to the system. Suppose we can observe the output of the system $f(x) = y$, and we want to use the observed variable y to learn the hidden variables $\boldsymbol{x_o}$ such that $f(\boldsymbol{x}_o) = y_o$. To do this, we define a lease square's function $J(\boldsymbol{x}, y)$, as shown in equation 17

$$\min(J = |\boldsymbol{f}(\boldsymbol{x}) - \boldsymbol{y}|^2) \quad (22) \qquad (17)$$

The non-linear algorithm shown below can be used to find the value of $\boldsymbol{x_o}$

Iterative Non-Linear Least Square's Solver

- Given **y**
- Make initial guess for $n \times 1$ vector $\boldsymbol{x}_i$
- Error vector $\boldsymbol{e} = \boldsymbol{f}(\boldsymbol{x}_o) - \boldsymbol{y}$
- $while\left(\frac{1}{2}\boldsymbol{e}^T\boldsymbol{e} < \epsilon\right)$
    - $\widetilde{\boldsymbol{b}} = \boldsymbol{b} - \boldsymbol{f}(\boldsymbol{x})$
    - $\tilde{A} = \frac{\partial \boldsymbol{f}}{\partial \boldsymbol{x}}$
    - $\Delta\boldsymbol{x} = \left(\tilde{A}^T\tilde{A}\right)^{-1}\left(\tilde{A}\right)^T\widetilde{\boldsymbol{b}}$
    - $\boldsymbol{x} = \boldsymbol{x} + \Delta\boldsymbol{x}$
    - $\boldsymbol{e} = \boldsymbol{f}(\boldsymbol{x}) - \boldsymbol{y}$
- End

Figure 11: Iterative Non-Linear least square's Optimization algorithm

One advantage to this algorithm versus the steepest descent, is the ability to stack multiple observations $\boldsymbol{y} = \begin{bmatrix} y_1 \\ \vdots \\ y_k \end{bmatrix}$ and dynamically update the estimates $\boldsymbol{x}_o$ as new observations are made.

III.B.2 Clustering

For any kind autonomous RSA to operate intelligently, it needs to gather data from the environment, subsequently make inferences and conclusions from sparse and possibly incomplete data. Instead of pre-defining theoretical models to classify data based on how it 'should' fit (i.e., this stiffness matrix should represent a planar constraint, based on our geometric model), there are a number of statistical methods available for recognizing patterns and classifying data automatically [30], including Principle Component Analysis (PCA) and Bayesian Networks. In this work however, we focus on Clustering.

Consider a data set, such as points on a 2-dimensional graph (figure 12). By visual inspection, it is clear that there are two distinct groups within the whole population.

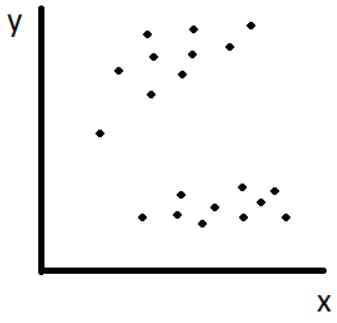

Figure 12: Illustration of Clusering

In the language of clustering, each individual point/measurement is called an 'Example' e, and each example has a feature vector $[X_1, X_2 \ldots X_m]$ (x and y values) with m elements ($m = 2$ in this case). In *hard clustering*, we wish to organize and classify this data set into k groups called *classes* (ideally 2 groups in this case) which share similar feature vectors.

One simple algorithm to do this is called the **k**-means algorithm, which is initialized by randomly assigning one of k classes to each example (a random classification), and then iteratively improves this classification by minimizing the following utility function

$$\min\left(\sum_{e\in E}\sum_{j=1}^{m}\left(pval\left(class(e), X_j\right) - val\left(e, X_j\right)\right)^2\right) \qquad (18)$$

Where $class(e)$ is the class that was assigned to example e, $pval(class(e), X_j)$ is the mean value of feature vector element X_j for all the examples in$class(e)$, and where $val(e, X_j)$ is just the value of X_j in the feature vector of element e.

In words, this utility is just the sum of squares error between each of the examples e and the class they were assigned to. This utility function results in good classifications, in which classes would be comprised of similar examples, such that the mean value for each class is close to the actual value of any particular example within that class. The k-means algorithms iteratively improves the classification at each step by re-assigning each example to the cluster which best fits it, using the mean value of the cluster in the previous step.

Eventually, the k-means algorithm will reach a stable classification (a local minimum of the utility function), which can be used to making decisions / inferences / predictions about current and new data points. This simplified algorithm is only a local optimizer, and is not guaranteed to find the optimal classification of the data set (the global minimum of CU). With n data points, and p possible classes, there are p^n possible classifications, the optimal classification problem is exponential in its run time. Furthermore, the optimal classification problem can be shown to be NP complete, as the CNF Satisfiability problem (a known NP-complete problem) can be reduced to an instance of this problem.

III.B.3 Stochastic methods

In the absence of a structured model of a system, such as a clearly defined $f(\boldsymbol{x})$ or set of continuous variables $\boldsymbol{x}$, non-derivative based stochastic methods can be used to model/describe/predict the behavior of complex systems.

III.B.3.a Markov Models

Consider an abstract mathematical model of a system, in which the system can be in one of a finite number of states at any given time. This is called a state machine, and it describes the transition of the system from one state to another. They system could be as simple as a daily commute (see Fig. 13), in which the states are “At Home” (H), “In the Car” (C), and “At Work” (W).

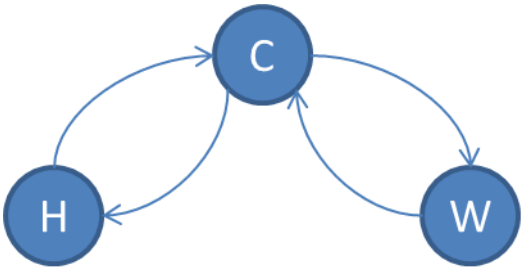

Figure 13: State Machine

The home state will always transition to the car state, before transitioning to the work state, with the same being true in reverse.

Markov models are stochastic versions of state machines, and are used to model non-deterministic systems through probabilities. A possible example of a Markov model is the following Markov chain (Fig. 14), which describes the weather on any particular day, with states “Sunny”, “Cloudy” and “Rainy”, and the probabilities of the next day’s weather given today’s forecast.

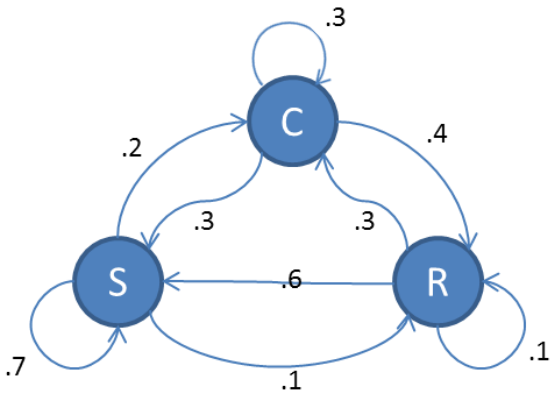

Figure 14: Markov Chain

Using experience from previous weather patterns (specifically, via a state transition matrix), it is possible to determine the probabilities of these state transitions, and predict future weather patterns, or infer previous weather patterns, given the current state.

One example of the use of Markov Models can be seen in Rosen et al (2006) [40], in which a generalized minimally invasive surgical procedure was broken down into a set of discrete, elementary subtasks (such as clamping, gripping, etc..). These sub-tasks were then represented as states in a Hidden Markov model (HMM), and each state was associated with a certain end effector motion/force profile. Given a set of training data, the HMM could then be used to guess the current surgical subtask being performed by a surgeon, by stochastically estimating the current state of the Markov model. Another example of Markov chains would be the Random Walk algorithm, as discussed below.

III.B.3.b Random Walk

Like a Markov model, random walks are stochastic models that are often used to describe systems. In the context of Numerical optimization, random walks can be used as a method of escaping local minima. Given an n-dimensional space, with a state $X = \{x_1, x_2 \dots x_n\} \in \Re^n$, a random walk is simply a sequence of s random steps in n-dimensional space, from the current state to some new state.

$$x_i = x_i + \sum_{t=1}^{s} rand(t) \qquad \forall x_i \in X \tag{19}$$

$$rand(t) \sim U(-\Delta x_i, \Delta x_i) \tag{20}$$

$U(x, y)$ here is random uniform distribution from x to y. Random walks can be used not only to escape local-minima, but to add a level of non-determinism into an

otherwise fairly deterministic algorithm, such as the gradient and Quasi-Newton algorithms presented above. In the best case, a random walk will only create deviations on the path to the correct solution. In the worst case however, a random walk can help avoid traps/ relapses into local minima

III.B.3.c Monte-Carlo methods:

The non-linear/gradient optimization methods presented previously are "greedy" derivative based optimization methods. Greedy algorithms, algorithms which blindly follow locally optimal trajectories without considering alternative steps/paths, often run into issues of local minima. For high parameter spaces and complex non-linear functions $f(x)$, such as might be found in solving for unknown parameters of a system f, the problem of local minima can become fairly prohibitive in finding an optimal solution to the problem. Monte-carlo methods lie within a larger class of derivative free and often population based optimization methods, many of which can be efficiently used to solve problems in highly non-linear, discontinuous and large-parameter spaces.

These are stochastic optimization methods, and operate in the following way:

1. Given an n-dimensional parameter space $X = \{x_1, x_2 \dots x_n\} \in \Re^n$
2. Then create a number of samples over the parameter space
3. These samples are evaluated in terms by some deterministic metric $f(\boldsymbol{x})$
4. These results are then aggregated to determine a solution.

An example application of a Monte-Carlo method would be as follows: Consider a system with a set of parameters $\{x_1, x_2, x_3, x_4, x_5\}$ in which x_1, x_2 and x_3 are known, while x_4 and x_5 are inherently unknowable/unobservable. The combination of these

parameters can deterministically yield one of two implications: M and M'. A Monte-carlo method could be used to search the parameter space of x_4, x_5 by creating a set of samples of these parameters. Each sample of x_4 or x_5 can be evaluated by their likelihood of being the value of x_5. The aggregate can then be used to evaluate the probability of M or M', given unknown values of x_4 and x_5..The complexity of such problems are exponential with the number of unknowns n, such that given domain size p, the run-time scales with p^n. While Monte-Carlo methods can help stochastically explore a large domain, it requires prohibitively higher (exponential) number of sample points as the dimensionality of the problem increases.

III.B.3.d Particle Filtering

Other stochastic population methods, such as Genetic Algorithms and Simulated annealing, perform an optimization to find optimal configurations of $\boldsymbol{x}$. Particle filtering is a simple and easy to implement stochastic optimization methods. The algorithm proceeds as follows:

1. Create a large set of m samples of an n-space, called ‘particles’
2. Assign them random values in the n-dimensional space
3. These particles are assigned some fitness metric
4. These fitness metrics should be weighted to a probability (0-1) such that, the higher the metric, the higher the probability
5. This will be the probability that this particle will not be eliminated after ‘filtering’
6. ‘filtering’ selects each particle and may delete it, based on its probability
7. New particles are added to the population and the process is repeated

This and the other population based algorithms seek to stochastically weed out un-optimal configurations of $\boldsymbol{x}$, while iteratively and randomly altering $\boldsymbol{x}$ to find optimal configurations. Of course, as with any optimization algorithm, its performance highly depends on the chosen fitness function. An example of such an approach can be seen in Petrovskya's work [35], in which particle filtering was used to estimate the position and orientation of an object being grasped by an industrial robot. Given the geometric model of the object to be manipulated, as well as sparse tactile data (locations of contact, and surface normals), her stochastic methods generated a large set of possible solutions and weeded out those solutions which did not fit the geometric models. In the indeterminate case (infinitely many solutions), the algorithm returned a band of candidate positions/orientations of the object given the data set which had been collected, whereas deterministic solution methods (steepest descent) would have failed to properly reach such a set of solutions.

CHAPTER IV

IV PATH PLANNING FOR SAFE MANIPULATION

Given the problem statement in section I, any autonomous intelligent RSA will need to make decisions about how to safely move around within an unknown elastic workspace, without *a priori* information about the workspace. The RSA also needs to explore the workspace and gather more information in order to make intelligent decisions about how to move. The problem is, how do you safely manipulate an object with no *a priori* knowledge of the system?

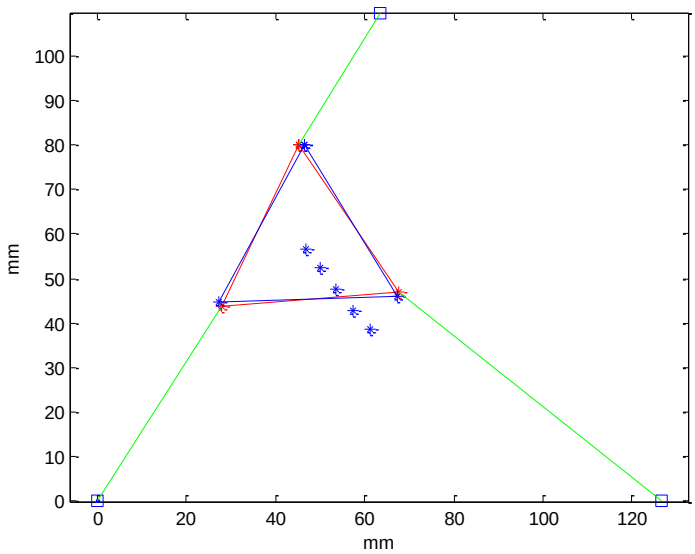

Figure 38: Planar Simulation of Object Manipulation

Given a gripper with an attached force sensor, we assume the elastic wrench $\boldsymbol{w}_e$ on the gripper and the gripper pose $\boldsymbol{\zeta}$ are immediately available at every time step. Consider these the states of the system. In addition, the directly obtainable states can be

used to deduce the Stiffness and Elastic energy, which are the spatial derivatives and integrals of $\boldsymbol{w}_e$ respectively. Even without *a priori* knowledge, the RSA can make intelligent decisions using not only the currently available states, but on deduced states as well. This will allow the RSA to manipulate an object towards a goal configuration.

First, we want an RSA to make decisions that will: 1) get it to the goal configuration, 2) minimize distance taken to get to the goal configuration, 3) minimize the elastic energy displaced on the system and *most importantly* 4) avoid exceeding a specified set of hard constraints. To do this, a set of cost/reward functions can be defined, which are functions of the states of the system, and will reward the desired states, while penalizing undesired states.

A numerical optimization method (section III.B.1) can then be used to search the pose space $\boldsymbol{\zeta}$ for the configuration $\boldsymbol{\zeta}^*$ which minimizes $f(\boldsymbol{\zeta})$.

IV.A Function definitions

To formalize this, define a reward function "task" function t(x) to promote goal-seeking behavior, and a constraint "penalty" function c(x) to enforce the given constraint. These functions are defined below:

IV.A.1 Tasks

To enforce the goal-seeking behavior, define reward function $task = f(\zeta, \boldsymbol{w_e}, \boldsymbol{K}, E)$. To achieve the simple objective of moving a flexibly suspended object to

some goal pose $\boldsymbol{\zeta}_g$, we can mathematically express this task function as the square of the dimensionally weighted distance :

$$task = \boldsymbol{\zeta}_d^{\boldsymbol{T}} \Gamma_7 \boldsymbol{\zeta}_d \tag{21}$$

Where $\boldsymbol{\zeta_d}$ is the distance from the current pose to the goal pose, with the first 3 elements as the distance in Cartesian space, and the last 4 elements as the relative orientation $\delta\hat{\boldsymbol{q}}$ in quaternion space.

$$\zeta_d = \left[\left(\boldsymbol{r}_g - \boldsymbol{r}\right)^T, \delta\hat{\boldsymbol{q}}^T\right]^T \tag{22}$$

As shown in [42], the vector portion of $\delta\hat{\boldsymbol{q}}$ can be used as a metric for orientation error. Thus, we use the 7-dimensional matrix $\boldsymbol{\Gamma_7}$ to extract and weight the vector portion of $\delta\hat{\boldsymbol{q}}$ by α.

$$\delta\hat{\boldsymbol{q}} = \hat{\boldsymbol{q}}^{-1} * \hat{\boldsymbol{q}}_g \tag{23}$$

And $\boldsymbol{\Gamma_7}$ is a diagonal weighting matrix

$$\boldsymbol{\Gamma}_7 = diag(1,1,1,0,\alpha,\alpha,\alpha) \tag{24}$$

Here, $*$ designates the multiplication operator in quaternion space [43]. The scalar α is a dimensional weighting factor, to resolve the scaling between rotation and translation. It is defined as the ratio of translation to rotation needed to produce equivalent amounts of elastic energy.

$$E_k = \frac{1}{2}k_x(dx)^2 = \frac{1}{2}k_\theta(d\theta)^2 \tag{25}$$

$$\alpha = \frac{dx}{d\theta} = \sqrt{\frac{k_\theta}{k_x}} \tag{26}$$

The scalar stiffness k_x and k_θ can be obtained from the Frobenius norm of the translational and rotational quadrants of K (A and D, see section III.A.3), respectively.

IV.A.2 Constraints

In order to enforce the soft and hard constraints outlined above, we define 3 different penalty functions, and combine them into one cost function, which we can call the constraint function.

IV.A.2.a Constraint 1

To provide some form of real optimization in the path taken to the goal, we define a soft constraint, which puts a penalty on the elastic energy applied on the system, by the gripper, relative to the initial undisturbed configuration. This constraint function can be defined as

$$constraint_1(\zeta, \boldsymbol{w}_e, \boldsymbol{K}, E) = \kappa E \tag{27}$$

where κ is some scaling factor, and E is the elastic energy, relative to the initial state. As mentioned before, the elastic energy at each node is not explicitly measured, but rather inferred from the integral

$$E(\zeta) = \int_{\zeta_i} \boldsymbol{w}_e(\zeta)^T d\boldsymbol{\xi} \tag{28}$$

$\boldsymbol{\xi}$ is the screw twist, and is an explicit function of, but not equivalent to the derivative of the pose $\boldsymbol{\zeta}$ (because the pose includes terms in quaternion space, while the twist is measured in pure 6-dimensional Cartesian space).

IV.A.2.b Constraint 2:

We define a second constraint function to enforce the hard constraint that the absolute elastic wrench exerted on the elastic system never exceeds a critical value $w_{\max}$. This can be mathematically defined as shown below:

$$constraint_2 = \frac{\rho}{(w_{\max} - |\Gamma_6 \boldsymbol{w}_e|)} \tag{29}$$

Where $\Gamma_6$is a 6-dimensional weighting matrix, and ρ is a scaling factor, and is proportional to the constraint's radius of influence. Plainly stated, this constraint enforces a harsh penalty (blows up to infinity) as the magnitude of the elastic wrench approaches the critical value $w_{\max}$.

IV.A.2.c Constraint 3

In order to deal with local minima and constraint violations, we can define a 3rd and final constraint, called the 'red flag' constraint. The purpose of this constraint is to avoid moving towards known problem configurations (red-flags), such as previously explored local minima, and locations of hard constraint violations. To do this, we create a simple repulsive field around each of these locations. This constraint function can be mathematically expressed as

$$constraint_3 = \sum_{r_i=r_1}^{r_m} \frac{\gamma}{\sqrt{\boldsymbol{\zeta}_{r_i}^T \Gamma_7 \boldsymbol{\zeta}_{r_i}}} \tag{30}$$

Where $\boldsymbol{\zeta}_{r_i}$ is the relative position of the i^{th} red flag to the pose, and γ is another scaling factor, which is proportional to the radius of influence of the constraint.

The total constraint function is just the sum of the individual constraint functions (eq. 20).

$$Constraint = constraint_1 + constraint_2 + constraint_3 \tag{31}$$

The combined constraint function captures the penalty-avoiding behavior of each of the individual functions.

IV.A.3 J function

Lastly, we can define the J function, which is the sum of all the task and constraint functions:

$$\boxed{J = \sum tasks + \sum constraints} \tag{32}$$

Ultimately, the steepest descent optimization algorithm will seek to minimize the J function, in order to find a low-cost path to the goal, while observing the given set of constraints, by numerically evaluating the gradient of this function at every step.

To actually command the desired manipulator motion, the algorithm calculates the direction vector $\hat{\boldsymbol{p}}_{\boldsymbol{k}}$, at the k^{th} step of the algorithm.

$$\hat{\boldsymbol{p}}_{\boldsymbol{k}} = -\frac{\nabla J}{|\nabla J|} \tag{33}$$

Finally, the desired manipulator twist $\boldsymbol{\xi}_{\boldsymbol{k}}$ is set to be some scalar speed v_k in the direction of $\hat{\boldsymbol{p}}_{\boldsymbol{k}}$.

$$\boldsymbol{\xi}_k = v_k \, \hat{\boldsymbol{p}}_{\boldsymbol{k}} \tag{34}$$

This desired twist can then be sent directly to a resolved rates algorithm to achieve the desired manipulator motion for moving a flexibly suspended object.

Using the above functions with the steepest descent algorithm yields a basic but effective path planning algorithm for autonomously reaching the goal state. There are, however, a few things that need to be explained, and a few augmentations that need to be made, in order to make the algorithm practical.

IV.B Algorithm Augmentations

IV.B.1 Dynamic Updating

At every step, the quantities of ∇J and K need to be re-evaluated. The former is a gradient of functions of the four states, and the latter is the hessian of the elastic energy (gradient of the elastic wrench). In a very basic implementation of this algorithm, these derivative quantities could be explicitly evaluated via their respective derivative definitions: by perturbing the manipulator along each dimensions, and measuring the changes in J and $\boldsymbol{w}_e$.This implementation is time intensive, as it requires 7 additional manipulator movements every time the quantities need to be updated.

It is possible, however, to update both of these quantities at each step, without explicitly evaluating the derivative. The Broyden-Fletcher-Goldfarb-Shanno (BFGS) [29] method comes from numerical optimization, and provides a way of estimating and updating the hessian of a function, using only rank-1 gradient information. The formula for BFGS is shown below

$$\boldsymbol{B}_{k+1} = \boldsymbol{B}_k - \frac{\boldsymbol{B}_k \boldsymbol{s}_k \boldsymbol{s}_k^T \boldsymbol{B}_k}{\boldsymbol{s}_k^T \boldsymbol{B}_k \boldsymbol{s}_k} + \frac{(\boldsymbol{y}_k \boldsymbol{y}_k^T)}{\boldsymbol{y}_k \boldsymbol{s}_k}$$

Where B_k is the hessian function of $f(\boldsymbol{x})$, y_k is the change/gradient of the function ∇f, and s_k is the change in the domain of the function, $\Delta \boldsymbol{x}$. For our application, we can set the function to the elastic energy of the system $E(\boldsymbol{\zeta})$. The gradient ∇f then becomes the measured wrench $\boldsymbol{w}_e$, and s becomes the infinitesimal twist from the previous step to the current step $\delta \boldsymbol{\xi}_k$.

This formula will make rank-1 updates of the stiffness matrix, by evaluating the change in wrench only along the path of travel. While this necessarily loses information over-time about directions not along the trajectory, this lost information is arguably not as important. Additionally, there are measures available, including minor randomization to the trajectory, to recover lost information about the stiffness in full 6-dimensional space.

Secondly, given K which is updated at every step with BFGS, it should be noted that the other 3 states can be integrated from position. That is,

$$\delta \boldsymbol{w}_e = K\delta\boldsymbol{\xi}\,,\ \delta E = \boldsymbol{w}_e\delta\boldsymbol{\xi}\ ,\ \delta\boldsymbol{\zeta} = f(\delta\boldsymbol{\xi}) \tag{35}$$

Since J is explicitly only a function of $J = J(\boldsymbol{w}_e, E, \boldsymbol{\zeta})$, it's derivative can be evaluated without actually perturbing the system.

$$\nabla J(\boldsymbol{\zeta}) = \frac{J(\boldsymbol{\zeta} + \delta\boldsymbol{\zeta}, E + \mathbf{w_e}\delta\boldsymbol{\xi}\ ,\ \boldsymbol{w_e} + K\delta\boldsymbol{\xi}) - J(\boldsymbol{\zeta}, E, \boldsymbol{w}_e)}{\delta\boldsymbol{\xi}} \tag{36}$$

Using these methods, it is possible to update and estimate ∇J and K at each point on the trajectory, without making any deviations/perturbations.

IV.B.2 Path discretization

To facilitate storage of data into memory (storing path histories at 1kHz is impractical), as well as in updating derivatives ΔJ, K, the path/ path history of the manipulator is discretized from a continuous curve to a set of nodes. This is done by determining the next node n_{k+1} by calculating $\boldsymbol{\zeta}_{k+1}$ along $\hat{\boldsymbol{p}}_{\boldsymbol{k}}$, and then moving along $\boldsymbol{\xi} = v_k\,\hat{\boldsymbol{p}}_{\boldsymbol{k}}$ until $\boldsymbol{\zeta} = \boldsymbol{\zeta}_{k+1}$.

IV.B.3 Backtrack algorithm

One flaw of using an optimization algorithm like this is the susceptibility to local minima. Another problem is how to deal with constraint violations. To solve these

problems, a 2-part solution is implemented: Red-Flag nodes, and Backtrack/random Walk algorithms.

As mentioned in the constraint function definition, we can label problem configurations, nodes at which local minima are detected or where there is a constraint violation, as a 'red-flag' nodes. Constraint 3 then creates repulsive fields around these red-flag nodes, so as to avoid visiting them again.

After labeling a red-flag, a backtracking algorithm can be used return along the recent trajectory to some previously explored node, and starting again. A random walk algorithm can also be implemented to add a level of non-determinism to the system, to avoid repeat configurations. To implement these solutions together, a simple Markov Chain was defined (see section III.B.3.a), to stochastically determine when and how-many backtracking /random walk steps should be made.

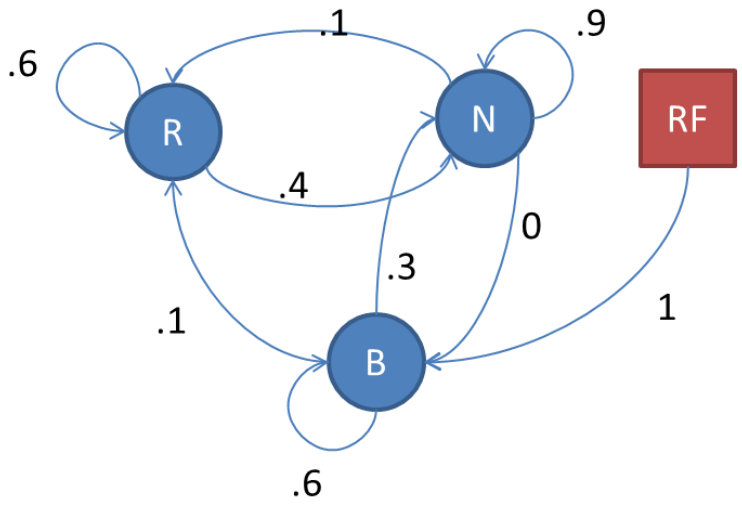

Figure 15: Backtrack Algorithm

The Markov Chain involves 3 states: the normal state 'N' ($\widehat{\boldsymbol{p}}_{\boldsymbol{k}}$ determines next node), 'R' which is a random step, and 'B' which moves one step back in the trajectory. Detecting a red flag automatically sets the state as B, and initiates backtracking. The transition probabilities were defined in order to achieve the following behavior:

- In the backtracking state, probability p of retaining the back-tracking state results in the algorithm backtracking a random number of steps, with an expected $\frac{1}{1-p}$ steps, and the probability of backtracking n steps being p^{n-1}. For 60%, this results in 2.5 expected steps. After backtracking, the algorithm will either enter a random walk, or the normal state.
- In the random walk state, the probability p of retaining the random walk state results in the algorithm performing a random number of random steps, with an expected $\frac{1}{1-p}$steps. Like the backtracking algorithm 60% results in an expected random walk of 2.5 steps. Once the random walk is completed, the algorithm will decay back into the Normal state.
- In the Normal state, the manipulator will follow its normal trajectory, and continue to do so with probability p at each node. With a 10% probability of retaining the normal state, the algorithm will move an expected 10 steps normally, before making a random walk.

IV.C Safe Manipulation Algorithm

With the functions and augmentations defined, we can finally present the safe-manipulation algorithm, shown in graphical form below (figure 16). At each regular step, the algorithm evaluates the gradient ∇J, and calculates the position of the next node to visit, and a twist-velocity to that node. Once the next node is reached, the algorithm is iterated, and the states are updated. Unless the MDP chooses a random walk, the algorithm will repeat itself and re-evaluate the gradient ∇J. It will repeat this procedure until it reaches the goal state (the distance to the goal falls below ϵ).

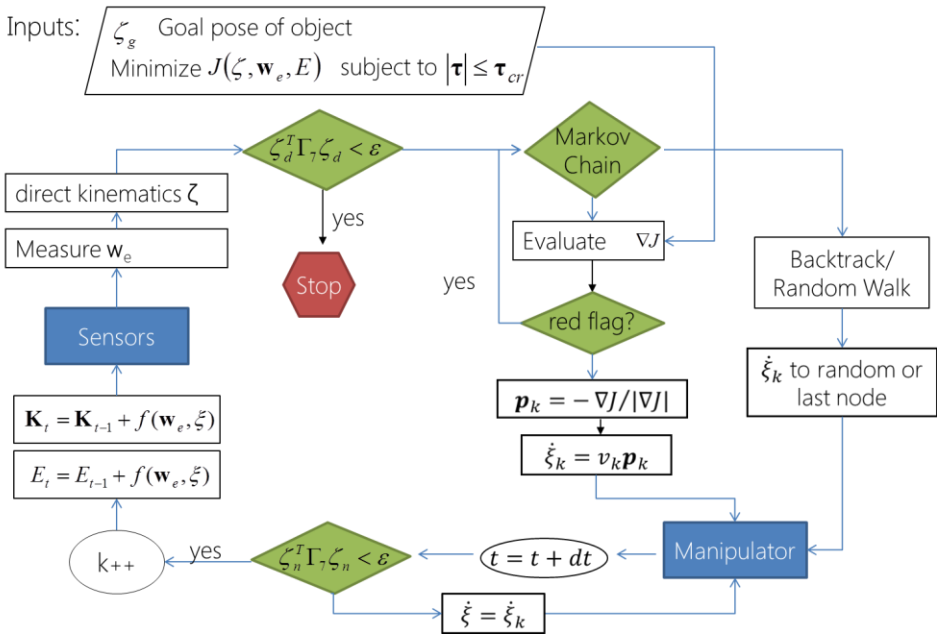

Figure 16: Safe Manipulation Algorithm

IV.D Simulation

Before experimentally testing the algorithm, it was implemented in simulation, using a simplified planar simulation (shown below, Figure 31). In this simulation, the object to be manipulated was a rigid planar triangle (red), attached by simple linear springs (green) to fixed locations the ground. A manipulator (not drawn graphically), is assumed to have perfect kinematic control over the red triangle $[x, y, \theta]$, as well as perfect force sensing capability $[f_x, f_y, M_z]$, and is commanded to move the red triangle from its initial configuration to some desired planar configuration (shown in blue).

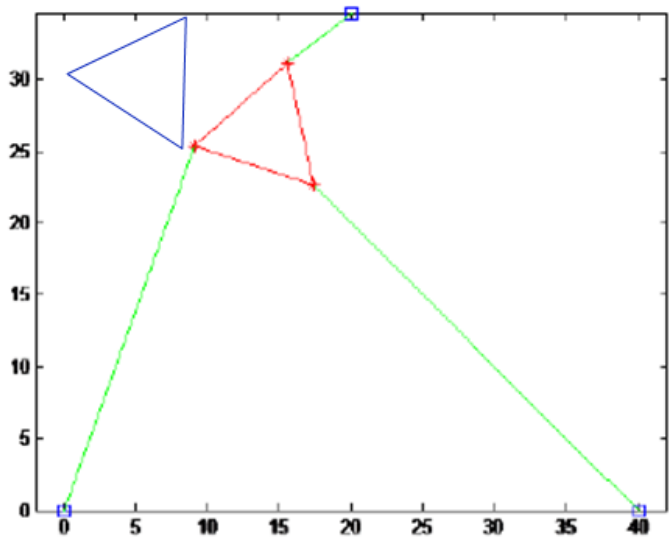

Figure 31: Planar Robot Simulation

In order to test the ability of the algorithm to converge on the desired configuration, two scenarios were presented. The first scenario involved setting the desired configuration of the rigid body to a configuration which would not violate any constraints. The other scenario was obviously to set the desired configuration to one that

clearly would violate the constraints if it was achieved. Below is the graphical output of the outcome of the first scenario.

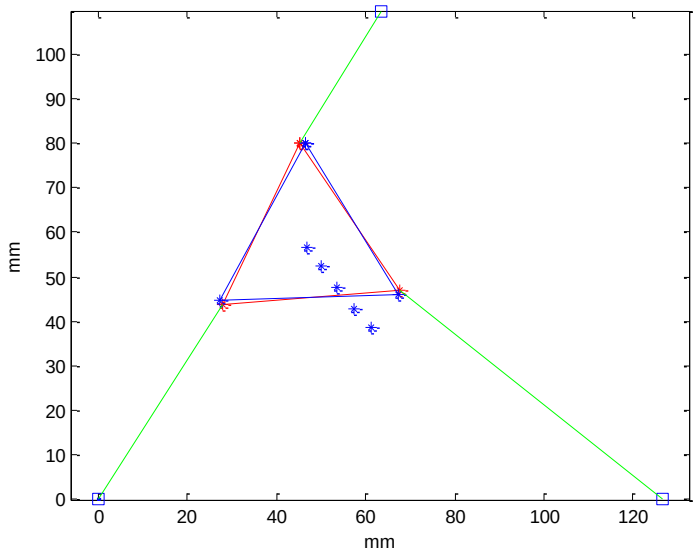

Figure 32: Planar Robot Simulation, Feasible goal

Here, the blue dots represent nodes that have been stored along the trajectory of the rigid body, and the blue triangle represents the desired configuration of the rigid body. Without any constraints near violation, the rigid body heads directly towards the desired configuration and converges without issue.

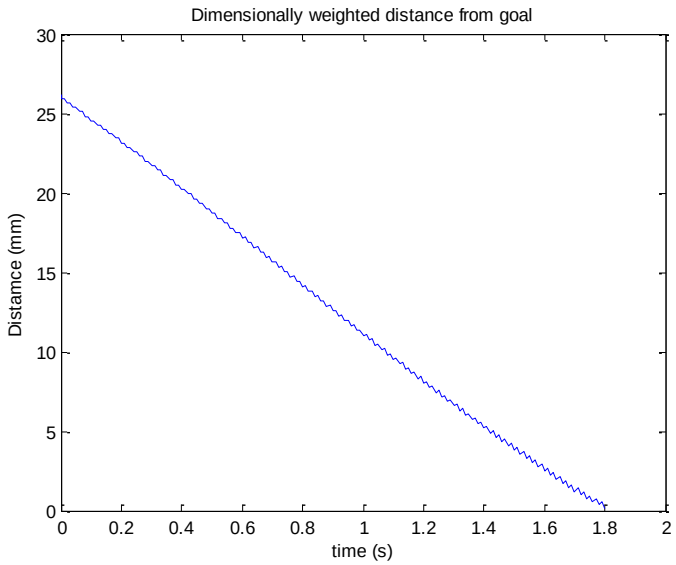

Figure 33: Error Profile, Feasible Goal

The error profile (distance to the goal) from this simulation is shown above in Figure 33.

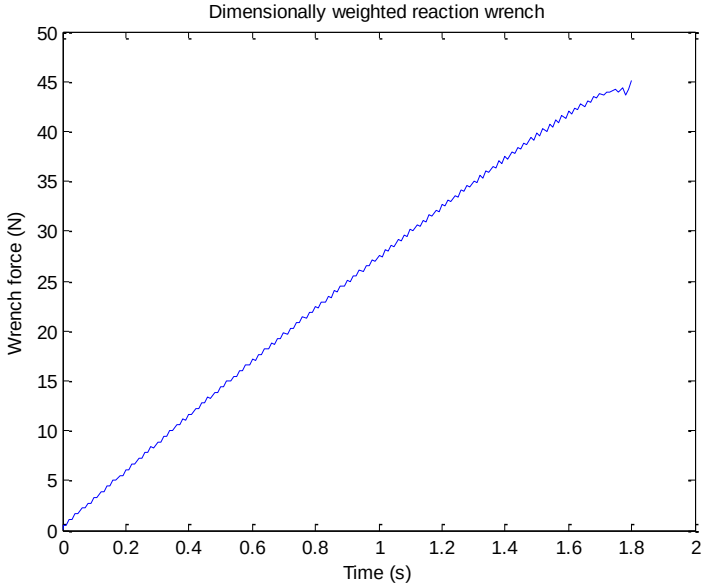

Figure 34: Wrench Profile, Feasible goal

The wrench profile for this simulation is shown above, in Figure 34. Given that the critical (dimensionally weighted) wrench is 50N, the desired configuration is still close to violating the primary constraint.

For the other scenario however, convergence was not possible since the desired configuration would have resulted in constraint violation. The graphic output of this simulation is show below:

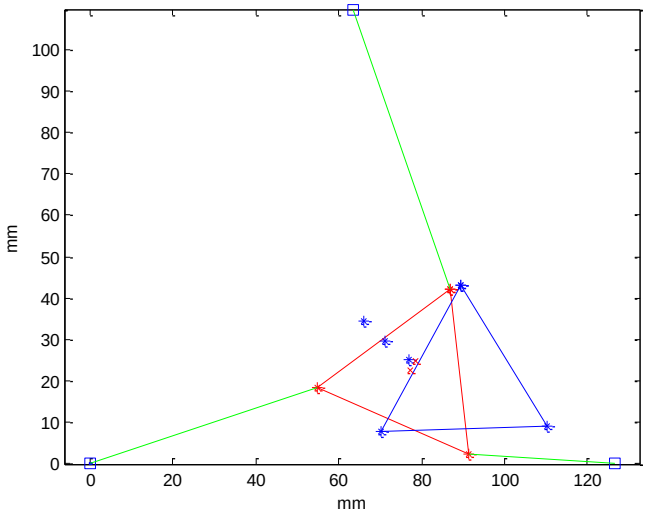

Figure 35: Planar Robot Simulation, Infeasible Goal

Here, the red stars represent red flags. It leaves red flags at the boundary between the constraint space and the freedom space.

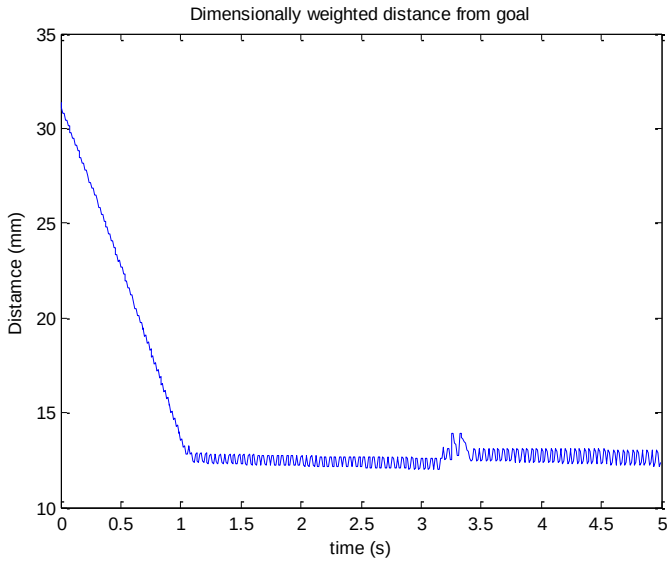

Figure 36: Error Profile, Goal

As shown in the distance profile in Figure 36, above, the rigid body attempts to get as close as it can to the goal, without violating the constraint. Eventually, the path planner sends it do a configuration which does violate the constraint at around 3.25 seconds, and the rigid body is returned to the nearest safe-point.

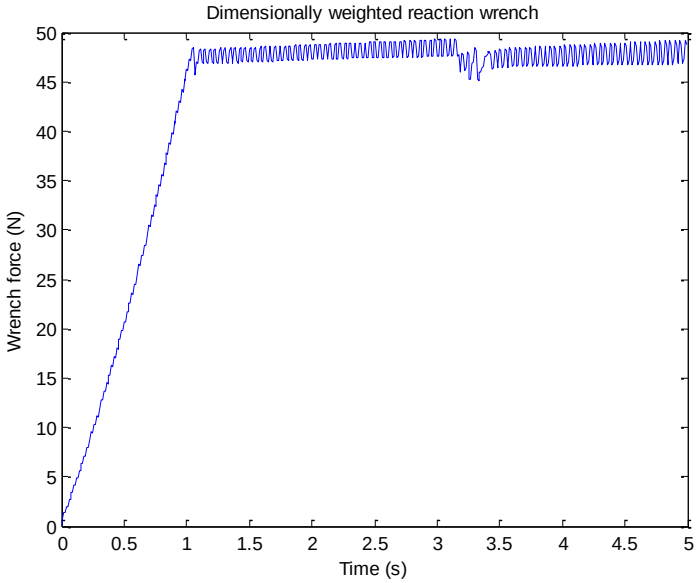

Figure 37: Wrench Profile, Infeasible Goal

The situation is clear when looking at the force profile in figure 37. Since the rigid body can't reach the desired configuration without violating the constraint, it hovers around a configuration which lies just below the threshold for constraint violation.

IV.E Experimental Evaluation

To test this algorithm experimentally, a simple experimental mock-up of an object, suspended in a flexible environment, was laser cut and assembled with springs, as shown in Figure 17 below. To manipulate this object, a Puma560 industrial robot was used, with a Gamma ATI 6-axis force sensor and a custom-made solenoid powered gripper, designed by the author for the purposes of these experiments and manufactured with a rapid prototyper.

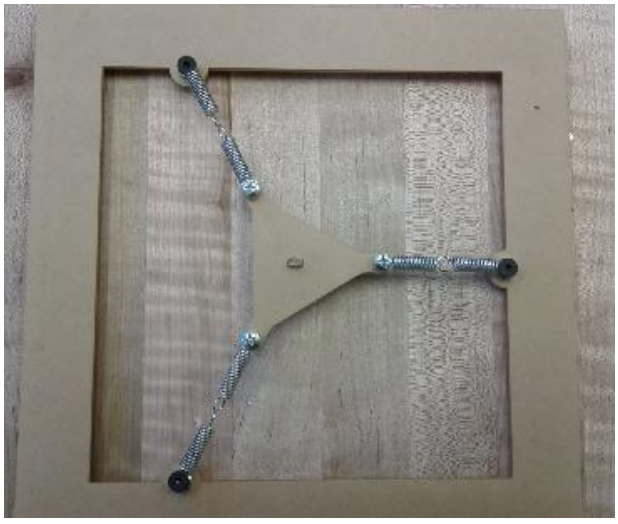

Figure 17: Rigid Triangle

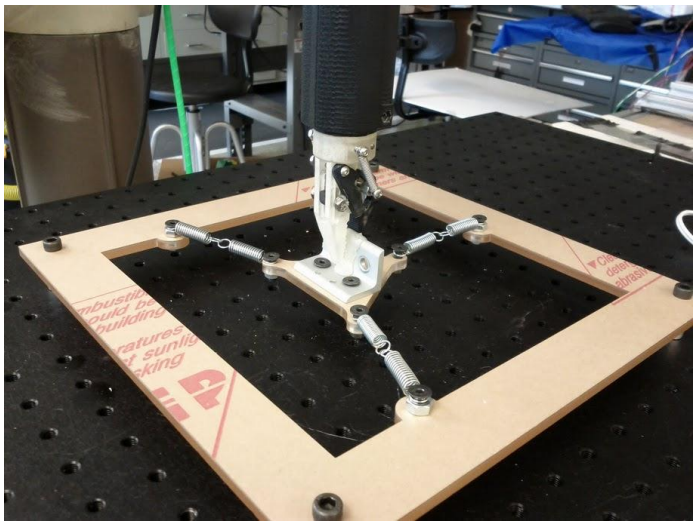

Figure 18: Safe Manipulation Setup

Given a target pose for the planar object, the autonomous manipulation algorithm was able to move the rigid triangle to the goal pose, or get as close as possible without violating the constraints. While this algorithm is elementary, it is important to emphasize its effectiveness and repeatability. The results from two such runs are shown in figures 19, and 20 respectively.

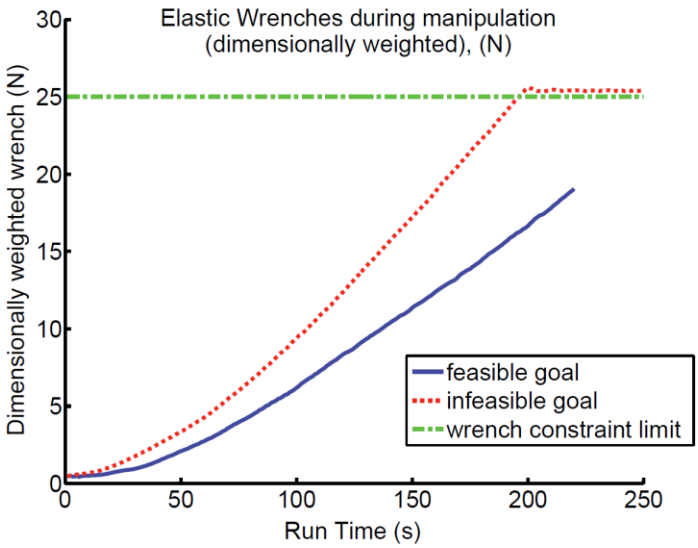

Figure 19: Autonomous navigation: Wrench profile

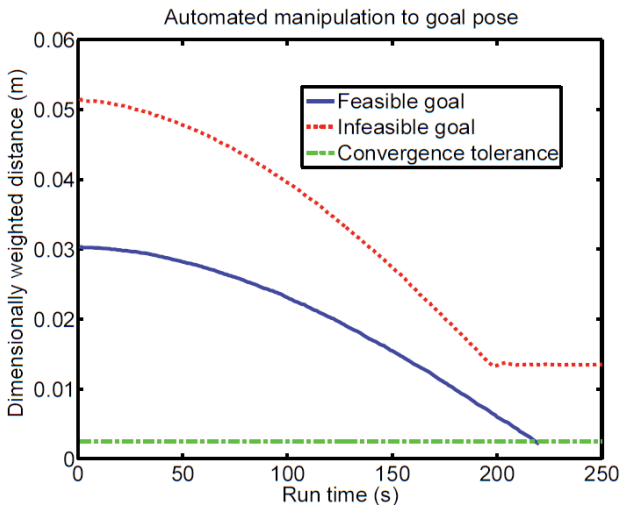

Figure 20: Autonomous navigation: Pose profile

In one of the runs, the goal pose $\boldsymbol{\zeta}_g$is $[.025, .02, 0]^T$, while the other has a goal pose of $[.035, .04, .0078]^T$. These poses are listed in planar coordinates ($[x, y, \theta]^T$) in units of [m, m, rad] respectively. In the latter run, the robot is prevented from moving to the goal pose, to avoid violating a maximum constraint force of 25 N. In this way, the constraint function acts like a basic virtual fixture, however it operates in the unknown force domain, as opposed to the spatial domain.

CHAPTER V

V CONSTRAINT DETECTION, CLASSIFICATION AND MAPPING

Finite element methods are currently the most popular method of representing global stiffness properties of elastic body/environment, and they do have their advantages. They allow complete and accurate description of the full workspace given the necessary parameters of the system. For the application of robotic surgery however, they are impractical. They require a-priori knowledge of the structure and parameters of the system, and as well as localization/registration to match the numerical model with real observed data during an operation. Most importantly however, they cannot be implemented in real time due to significant computational costs.

Ideally, there would be some method that makes no assumptions about the environment, (a blind algorithm), and perfectly describes the elastic behavior of the unknown system. In practice however, to describe the elastic behavior of the system, some information/properties have to either be assumed about the environment (not blind), or gathered and deduced from the environment during exploration. This work takes the latter approach, and presents an algorithm which makes no minimal about the nature of the environment, and uses only local stiffness information during exploration of the environment, and deduces/infers the global stiffness properties using a constraint based model. This allows compact representation of global elastic properties, using methods and calculations easily realizable in real time.

V.A Spatial Stiffness

Commonly, exploration algorithms (see Section II.B) use kinematic constraints to determine allowable directions of motion of a manipulator in an environment, and consider primarily rigid constraints of the form shown in Section III.A.2.

In this work, we consider the idea of flexible constraints, in which the rigid assumption is dropped, and the kinematic constraints are no longer applicable. Unlike a rigid constraint, a flexible constraint does not prevent motion in a given direction (kinematic constraint), it can only impede motion in that direction. An example would be a flexible wall versus a rigid wall. A rigid wall could be modeled as being infinitely stiff, and thus would have the analogous kinematic constraint that a hand cannot physically move into the wall/occupy space within the wall. For a flexible wall, the rigid assumption is dropped, and the kinematic constraint is no longer applicable. A hand touching a flexible wall could push into the flexible wall, given sufficient force to over-come the impedance of the wall.

V.B Stiffness region

We seek to develop a method for characterizing the global stiffness behavior of a specific elastic workspace. Even if we use local stiffness properties to deduce the mechanical constraints at a given location, there can easily be multiple mechanical constraints that operate at different locations throughout the workspace. To resolve this, we introduce a new concept, called a *stiffness region.*

Consider a given mechanical constraint, such as the gripper in contact with the wall, as shown in figure 21.

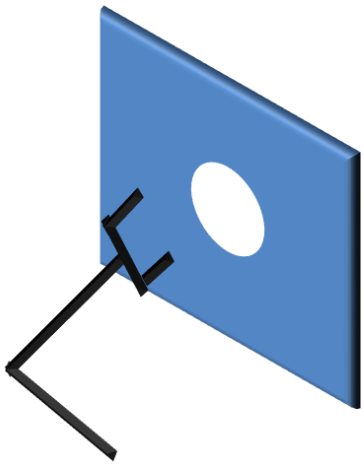

Figure 21: Stiffness Region example

- For a given system in which there is mechanical contact or coupling, which produces a specific mechanical constraint, there are multiply nearby configurations in which this coupling also exists and produces approximately the same basic mechanical constraint
- We define a 'Stiffness Region' Ξ as the set of configurations in which a specific mechanical coupling exists, and yields the same basic mechanical constraint

While the gripper of figure remains in contact with the wall, it is subject to a planar constraint, which prevents the gripper from moving into the wall. Thus any configuration that results in contact with the wall will be part of the same stiffness region Ξ.

If the gripper moves over the circular hole of the wall, however, the gripper will lose contact with the wall, and no-longer subject to the same set of constraints as it was before. The previous set of constraints have not disappeared, they are just not active at the new configuration of the gripper. The points on the wall and inside the hole can then be associated with two distinct stiffness regions, each of which exhibit a different set of mechanical constraints.

The global stiffness of an environment would then be composed not of an infinite number of local stiffnesses, but rather a finite number of identifiable stiffness regions. Each of these stiffness regions would then be a space, in which the local stiffness properties of every configuration in the space share the same form of elastic behavior/exhibit the same constraint. Using this definition, a stiffness region can be mathematically expressed as

$$\Xi \equiv \{\boldsymbol{\zeta} | \boldsymbol{\zeta} \leftrightarrow C\} \tag{37}$$

Where C is a mechanical constraint.

V.C Elementary Constraints

The question then becomes, how do we deduce mechanical constraints from local stiffness properties? This is done by considering stiffness itself as a type of constraint.

Consider the principle rotational and translational stiffness axes of a spatial stiffness matrix (see section III.A.3). The result is six vectors in space, each with a direction and a magnitude. Each of these vectors represents a possible direction of motion (rotational or

translational), and its associated eigenvalue represents the magnitude of the stiffness/impedance to motion along that direction.

Accordingly, these principle axes can each be thought of as 1 degree of freedom constraints, which impede motion along a given direction. We can call these 1 DoF constraints 'elementary constraints', and the superposition of these elementary constraints is the composite which describes the local stiffness. In fact, we can represent well known and theoretical common constraints (See section III.2.a) as the superposition of rigid elementary constraints.

Any of these theoretical mechanical constraints are simply a set of orthogonal elementary constraints, which are binary (rigid or free) and frame invariant (the relation between these constraints hold in any reference frame). The principle translational and principle rotational stiffness of $\boldsymbol{K}$ provide orthogonal sets of elementary constraints, whose magnitudes are numerically quantified and frame invariant.

Taking advantage of this equivalence, we therefore propose representing mechanical constraints, flexible or rigid, by the eigenvalues of the principle axes $C = [\sigma_1, \sigma_2, \sigma_3, \mu_1, \mu_2, \mu_3]$ of stiffness matrix K, where σ represents translational stiffness, μ represents rotation stiffness, and where each set is ranked in *descending* order. To denote this particular representation, we call the resulting vector of eigenvalues a *Constraint vector*, as shown in equation 38 below.

$$C_v = [\sigma_1, \sigma_2, \sigma_3, \mu_1, \mu_2, \mu_3] \tag{38}$$

To illustrate this, consider the rigid 2-D curved surface in Figure 22. There is essentially a rigid planar constraint for any local configuration on the curved surface.

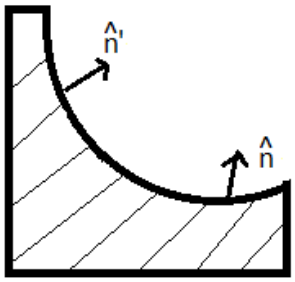

Figure 22: Frame invariant Constraint s: Normal vectors on a curved surface

For any configuration along the surface, the constraint can be represented as $C = C' = [\infty, 0, 0, \infty, \infty, 0]$, which is true for any perfectly rigid planar constraint, regardless of the direction of the normal to the plain.

To illustrate the process, consider the gripper in figure 23, below, in what shall be called a 'membrane constraint'. The gripper grasps the thin and flexible membrane, and perturbs it along all 6 cartesian directions to evaluate the local stiffness properties.

Figure 23: Real Membrane Constraint

The resulting local stiffness matrix K is shown below

$$K = \begin{bmatrix} 965.081 & 51.38 & 168.67 & -0.252 & -16.456 & 0.347 \\ 51.38 & 1173.3 & 11.197 & -10.00 & -0.258 & -1.18 \\ 168.67 & 11.19 & 411.89 & -4.02 & 11.90 & -1.43 \\ -0.252 & -10.00 & -4.02 & 0.589 & -0.133 & -0.27 \\ -16.45 & -0.258 & 11.903 & -0.133 & 0.852 & -0.077 \\ 0.3469 & -1.18 & -1.439 & -0.276 & -0.077 & 0.203 \end{bmatrix} \quad (39)$$

To obtain the principle axes, the matrix K is broken down into upper left, upper right and lower right sub-matrices. Units are in N/m, N/rad, Nm/rad respectively.

$$A = \begin{bmatrix} 965.081 & 51.38 & 168.67 \\ 51.38 & 1173.3 & 11.197 \\ 168.67 & 11.19 & 411.89 \end{bmatrix} \quad B = \begin{bmatrix} -0.252 & -16.456 & 0.347 \\ -10.00 & -0.258 & -1.18 \\ -4.02 & 11.90 & -1.43 \end{bmatrix}$$

$$D = \begin{bmatrix} 0.589 & -0.133 & -0.27 \\ -0.133 & 0.852 & -0.077 \\ -0.276 & -0.077 & 0.203 \end{bmatrix} \quad (40)$$

Using the approach developed in Lin [39] , the rotational stiffness matrix K_v and the translational stiffness matrix K_w are obtained from the sub-matrices, as shown below.

$$K_v = D - B^T A^{-1} B \qquad K_w = A \quad (41)$$

$$K_v = \begin{bmatrix} .4630 & .0207 & -.3018 \\ .0207 & 0 & -.0315 \\ -.3018 & -.0135 & .1967 \end{bmatrix} \quad K_w = \begin{bmatrix} 965.081 & 51.38 & 168.67 \\ 51.38 & 1173.3 & 11.197 \\ 168.67 & 11.19 & 411.89 \end{bmatrix} \quad (42)$$

To obtain the principle axes, an eigenvalue decomposition is performed on each matrix:

$$\sigma Z_v = K_v Z_v \qquad \mu Z_w = K_w Z_w \quad (43)$$

$$Z_w = \begin{bmatrix} -.27 & .9224 & .2755 \\ .0039 & -.2852 & .9585 \\ .9627 & .2605 & .0736 \end{bmatrix} \quad Z_v = \begin{bmatrix} -.45 & -.3102 & -.8371 \\ .613 & -.7892 & -.0374 \\ -.6491 & -.53 & .5457 \end{bmatrix} \quad (44)$$

$$\sigma = [1188.9, \quad 996.8, \quad 364.6] \quad \mu = [.6606, \quad 0, \quad 0\ ] \quad (45)$$

Where Z_v and Z_w are the resulting eigenvectors (principle axes) and μ, σ are the magnitudes of the principle rotational and translational stiffnesses respectively. Finally, the constraint vector is defined as

$$C_v = [1188.9, \quad 996.8, \quad 364.6, \quad .6606, \quad 0, \quad 0] \qquad (46)$$

As can be seen from the translational eigenvalues, there are two directions in which motion is restricted in roughly equal magnitude, whereas there is one direction in which motion is not impeded and negligible rotational stiffness in any direction. Therefore, it is clear to see that the stiffness matrix does represent a membrane constraint.

V.D Constraint identification and classification

After sufficient navigation of the elastic system, as described in section IV , we can assume set of previously visited nodes $\{n_1, n_2 \dots n_k\} \in N$, each with a stiffness matrix K_i and an associated constraint vector C_i. To classify these constraints vectors, we can use the k-means algorithm (see section III.B.2) to break the set of nodes (examples) into a set of similar classes. The number of classes will be the number of constraints in the system, and the set of nodes in each class will be defined as a stiffness region, for that class.

In order to adapt the k-means algorithm to this problem, several small augmentations need to be made. Firstly, each constraint vector C_i contains a set of translational stiffnesses, and a set of rotational stiffnesses, each with its own set of units. To scale/balance the units, the dimensional weighting factor α can be used (see section IV.A.1) to scale rotational stiffnesses, such that $C_i = [\sigma_1, \sigma_2, \sigma_3, \alpha\mu_1, \alpha\mu_2, \alpha\mu_3]$.

Furthermore, the k-mean algorithm assumes fixed number of classes, which is used as an input to the algorithm. In our application however, the optimal number of classes is unknown however, so we make the number of classes k a variable, and define the following modified utility function which we wish to minimize:

$$CU = \left(\sum_{e \in E} \sum_{j=1}^{m} \left(pval\left(class(e), X_j\right) - val\left(e, X_j\right) \right) \right) k^2 \qquad (47)$$

Here, run the k-mean algorithm for several values of k, and find the optimal classification from this set of classifications, and thus the optimal number of classes k. Finally, in comparing objects with rigidity of different orders of magnitude, we propose using a log scale, in order to properly define clusters between both rigid and compliant stiffnesses.

$$CU_{\log} = \left(\sum_{e \in E} \sum_{j=1}^{m} \left(\log\left(pval\left(class(e), X_j\right) \right) - \log\left(val\left(e, X_j\right) \right) \right) \right) k^2 \qquad (48)$$

This methodology for constraint identification is validated experimentally in section V.F on several test objects within the Puma 560's workspace.

V.E Constraint exploration algorithm

Given a manipulator, manipulating an object in an unknown flexible environment (see section I), the following algorithm with allow the manipulator to develop a constraint based map of the elastic properties of the system as it explores it. The algorithm is initialized by performing a local perturbation to obtain the local stiffness properties, and subsequently defining the first stiffness region. At each iteration, the stiffness is updated

and a principle axis decomposition using eq. (40-44) is performed on $\boldsymbol{K}$. The resulting eigenvalues (principle stiffnesses) are stored in the constraint vector for the current node for use in cluster classification. If sufficient nodes have been explored, the clustering algorithm will define/update the clusters. If a new cluster is defined, a new stiffness region is defined for the associated constraint, and is then associated with all nodes within the new cluster. The algorithm is shown in Figure 24, below.

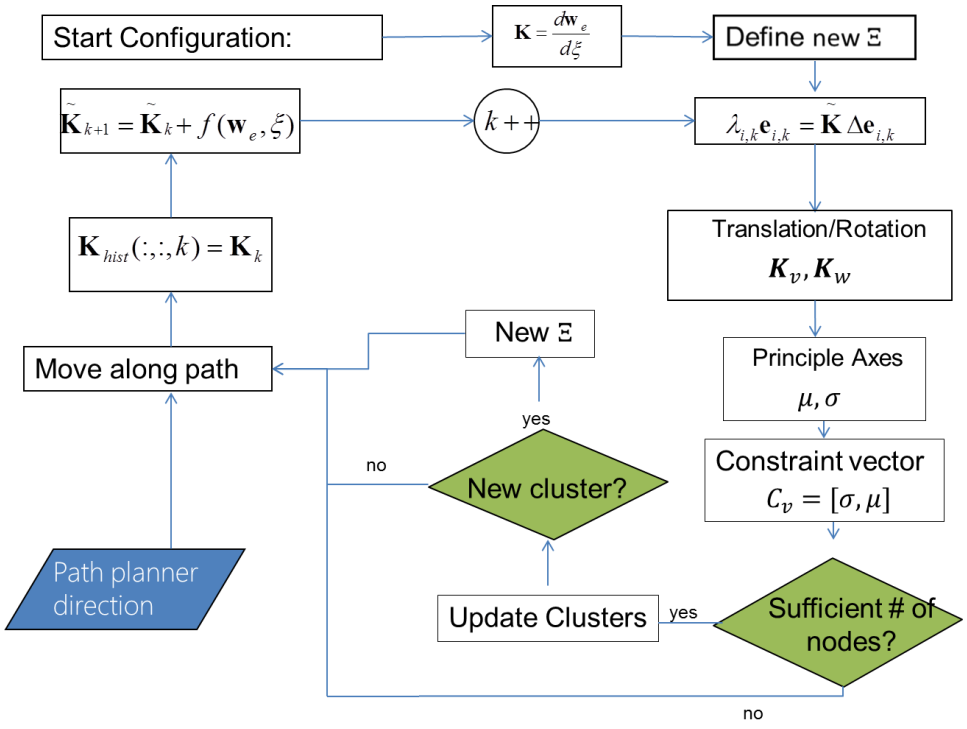

Figure 24: Constraint Exploration Algorithm, using Clustering and Stiffness Regions

V.F Experimental evaluation

In order to evaluate the proposed constraint detection/classification methodology, two series of experiments were conducted. The first used local stiffness

measurements to distinguish/classify the constraints represented by several different flexible objects. In the second experiment, the robot used local stiffness measurements to identify the constraint(s) and map the resulting stiffness regions over the surface of a single flexible object. These experiments were conducted using a Puma560 industrial robot arm, an ATI-Gamma 6 axis force sensor, and a solenoid-powered rapid-prototyped gripper, designed by the author for these experiments.

V.F.1 Constraint identification of multiple objects

In order to model several clearly distinct flexible constraints, 3 different mockups were created, each involving a flexible object constrained to the environment in a different manner, such that manipulation of the object had visually identifiable directions of compliance/rigidity. These objects, including a polyurethane flexible hinge, a foam sheet and a simple linear spring, are shown in figures 1a, 1b, and 1c below.

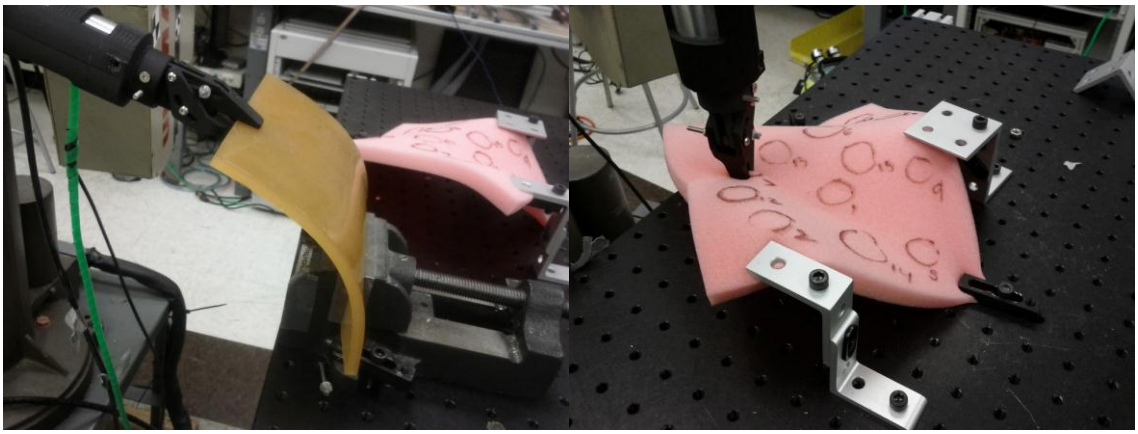

Figure 25a, 25b:Flexible Hinge, Foam Sheet experimental mock-ups

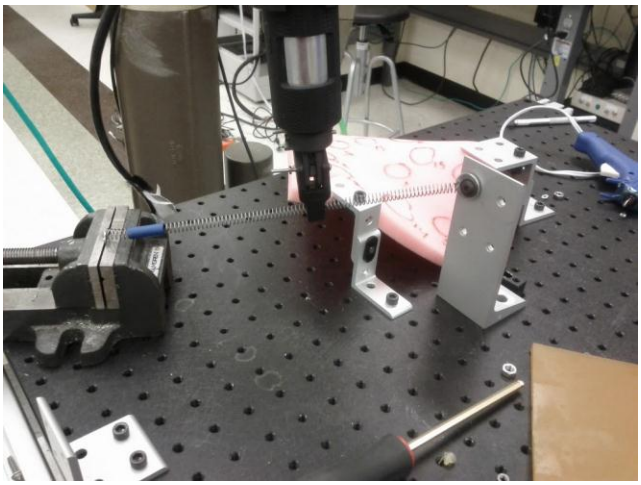

Figure 25c: Linear Spring Constraint

The robot was then used to grip each object at a point, and perturb it along each cartesian dimension to explicitly calculate the 6-dimensional local stiffness matrix. For each measurement, the object being manipulated was placed at a different configuration (different position and orientation, with respect to the environment), in order to emphasize the directional independence of this method. In total, 5 measurements were made for each object, with a total of 15 local stiffness measurements.

The resulting local stiffness matrices were decomposed into their principle axes, from which their constraint vectors (see equation 38) were obtaned. The constraint vectors were then fed into a clustering algorithm and automatically categorized into clusters, with the results shown (translational constraint vectors) in figure 26 below in semi-log scale.

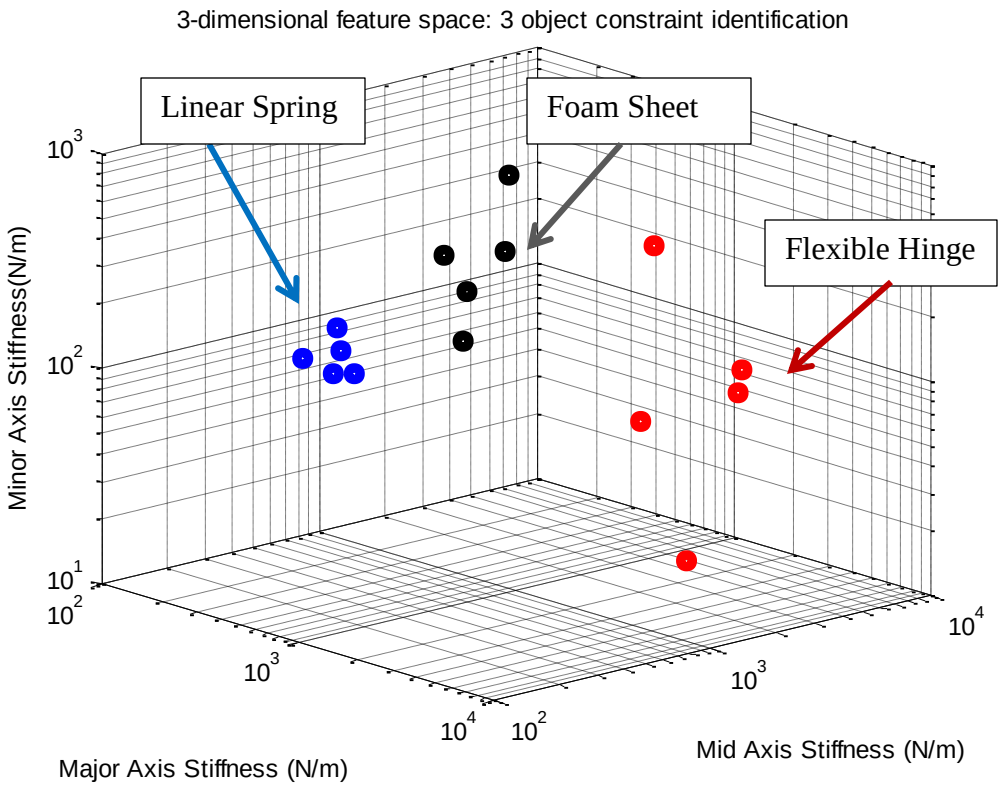

Figure 26: Constraint identification using clustering

The clustering algorithm broke the 15 measurements into 3 clusters (red, blue and black), correctly categorizing all 5 measurements corresponding to each object into its own cluster. The blue cluster corresponds to the linear spring, the red to the flexible hinge, and the black to the foam sheet. It should be noted that this clustering was obtained from the global optimal clustering (global minimum of $CU_{\log}$). This is important, as the traditional k-means algorithm (see section III.B.2) uses a local optimizer, whereas particle filtering (section III.B.3) was used here to find the global minimum.

The constraint vectors plotted in Figure 26 are shown below in tabular form, along with the average of their associated clusters.

Table II: Translational Constraint vectors obtained from local stiffness measurements of 3 different objects. All quantities are in units of N/m.

#	Linear Spring			Flexible Hinge			Foam Membrane		
1	729.32	195.39	137.3	6476.2	1121.5	22.05	776.79	752.96	241.40
2	656.98	222.50	213.49	4294.5	1151.6	565.44	847.42	548.86	398.12
3	613.99	163.75	161.37	6101.0	2154.4	142.95	1034.8	906.39	866.94
4	580.81	259.70	153.62	5689.7	2183.6	109.20	1037.6	860.99	391.49
5	751.12	233.90	133.76	4428.6	990.13	91.67	864.73	654.62	153.55
-	Average			Average			Average		
Av	666.44	215.07	159.92	5.39e+3	1.52e+3	186.257	912.28	744.77	410.3

V.F.2 Constraint mapping of a Foam membrane

In the second experiment, the local stiffness was measured at multiple locations along the surface of a pink foam sheet, attached to a rigid table by 4 separate clamps (shown in Figure 27 below). The nodes were manually distributed and marked, placing several nodes near the clamp attachment points where the foam's stiffness was noticeably higher.

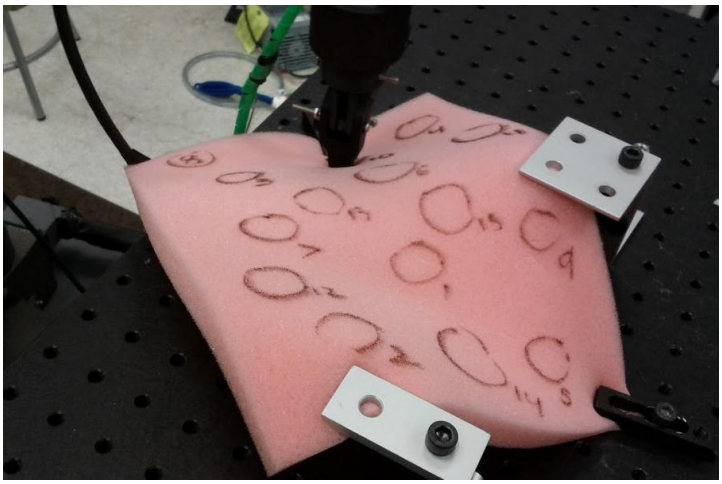

Figure 27: Foam Membrane Experimental Mockup

As with the previous experiment, the resulting local stiffness matrices were decomposed into their principle axes, and the associated constraint vectors were then fed into the same clustering algorithm, which automatically cateogorized the data into a set of clusters, as shown below (Figure 28).

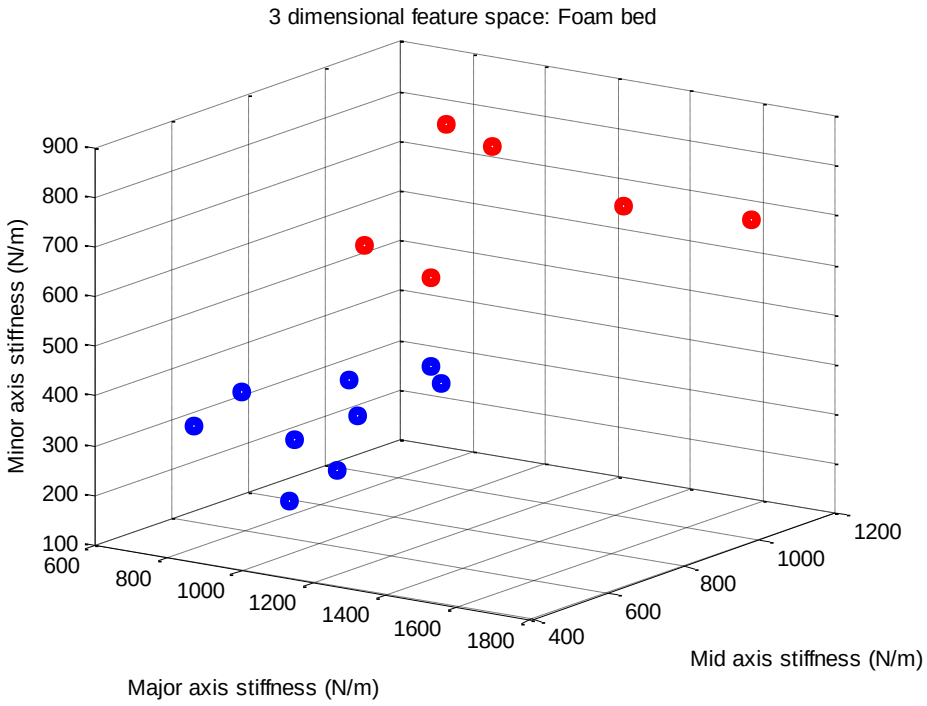

Figure 28: Constraint detection using clustering, Foam sheet

Using linear scale clustering algorithm [30] (as opposed to log scale), the algorithm identified 2 primary clusters, shown in blue and red. The blue cluster corresponds roughly to a membrane constraint, in which translation is impeded in a plane, whereas movement along the normal is fairly complaint. The cluster in red, however, corresponds to a more homogeneous stiffness, in which no axis in particular is negligible. There were two particular nodes in the middle, which were either one of the

two clusters in different non-optimal classifications, and which were assigned their own cluster in the 3-cluster classifications, however

Using the Cartesian position (all measurements were taken in the same orientation $q_o = [1, 0, 0, 0]$) of each node, and the classification obtained from the clustering algorithm, a 3-dimensional constraint map was defined for the foam sheet, and is shown below in figure 29.

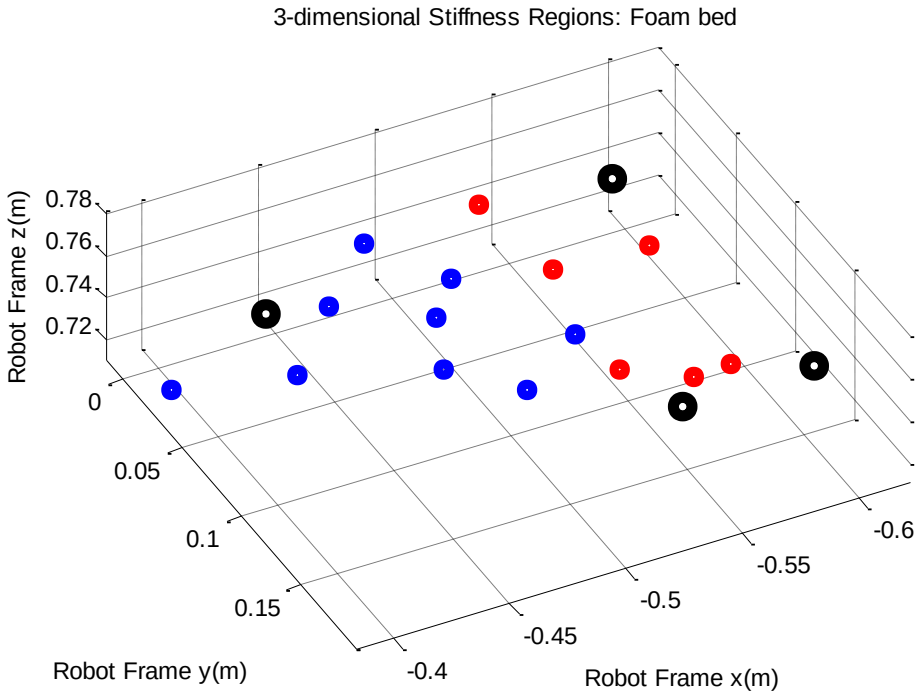

Figure 29: Constraint map, with Stiffness regions, of a Foam sheet

With two clusters identified, the nodes measured were broken into two stiffness regions, with red corresponding to higher rigidity, at nodes close to the clamps as expected. For comparison, the image of the actual foam bed is shown below in, figure 30

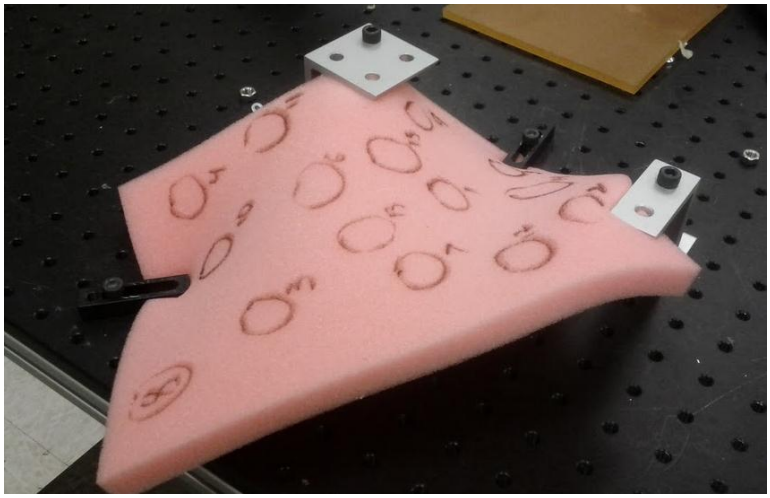

Figure 30: Foam Sheet Mock-up

V.G Discussion

The flexible objects used in these experiments were chosen as real examples of intuitive known constraints, in order to have a frame of reference for basic evaluation of the proposed constraint identification methodology. For this data set, the constraint identification clustering algorithm neatly and effectively partitioned the data set into sets of well-defined constraints, using only 3-dimensional vectors to describe the constraints.

While “membrane”, “flexible hinge” and “linear spring” constraints were chosen as intuitive theoretical models, there are many instances of these types of constraints in practice. Any thin-walled piece of tissue, such as the surface of the bladder, would exhibit a membrane constraint. The kidney, which has a series of tube connections along a line, creates a flexible hinge constraint. Finally, any organs constrained by single tubular connections, such as the appendix, will exhibit a “linear spring” constraint (linear

is a misnomer, as biological tissue can act as a spring, but whose properties are highly non-linear).

The flexible objects used varied greatly in scales of stiffness and the same is true of tissues within the human body. For a typical set of tissue, however, a rough idea of the stiffness is provided in the stress-strain diagram below, obtained from biomechanical references [45], [46]:

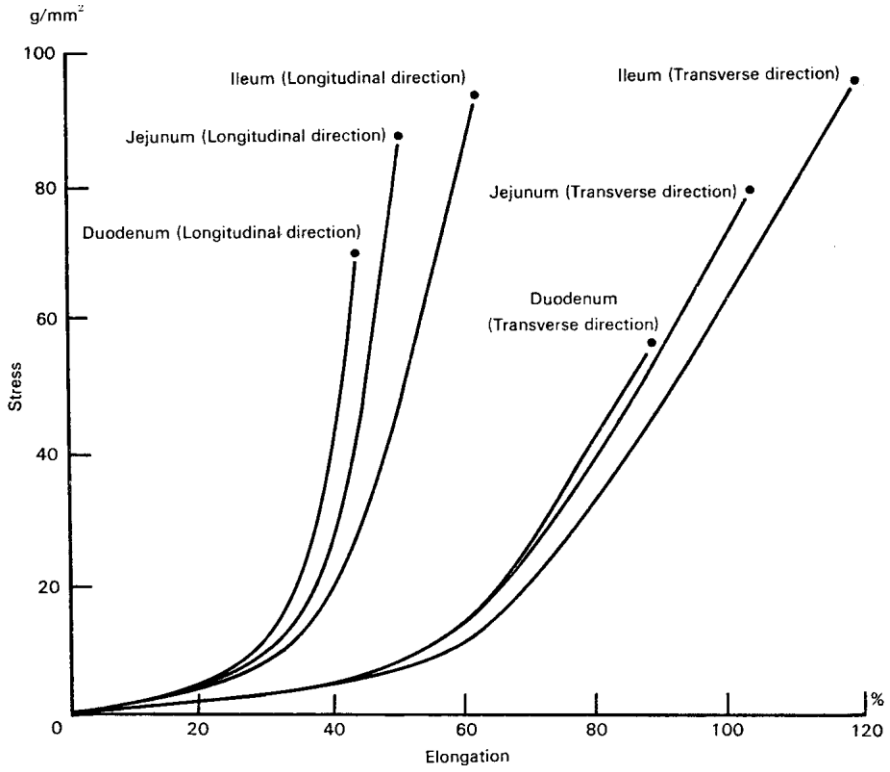

Figure 40: Biomechanical Tissue properties

Where the longitudinal stiffness for a tubular organ, such as the duodenum, would be around $8\frac{g}{mm^2}$ for small deformations. With a cross section area corresponding to a tube of $15mm$ diameter, and $50mm$ length, this would correspond to a stiffness of

$\sim 280 \frac{N}{m}$, which resides on the low side of the stiffness measurements founds in these experiments, however it is on the same/similar order of magnitude. Therefore, from the preliminary results, it would be safe to conclude that the presented constraint vector classification methodology is capable of identifying/differentiating between basic flexible constraints, using only local stiffness measurements. More thorough evaluation/performance analysis of these methods is left as future work.

CHAPTER VI

VI CONCLUSION

In this thesis, Algorithms for blind, safe, autonomous manipulation in unknown flexible environments were presented. A solution was proposed, using state-based cost/reward functions and force/based constraints/virtual fixtures, and was subsequently verified using a custom-fabricated planar mock-up of an elastic environment. Secondly, compact representation of global stiffness was presented via the use of stiffness regions and constraint maps, and real-time constraint detection/identification/classification was achieved using constraint vectors, 6-dimensional frame-invariant vectors derived from local stiffness measurements. These methods were evaluated using local stiffness measurements of several different flexible objects, each with its own constraint(s). A clustering algorithm was able to correctly classify/group together the stiffness measurements from 3 different flexible objects, and was furthermore able to define a constraint map, highlighting two distinct stiffness regions, over the surface of a particular flexible object.

Given the reasonable set of objects used in the constraint identification experiments, it would be safe to say that constraint vector clustering is at least capable of discerning/classifying constraints of basic flexible objects. The primary weakness of such a technique would be the situation of varied but smoothly changing stiffness properties, in which the constraint vectors would form a large continuous data set, and would result in poor cluster classifications. In such a situation, Principle component

Analysis might provide a much better framework for organizing/classifying the constraints. Using a log scale clustering however, the cluster technique is perfectly capable of discerning/identifying hard rigid constraints (bone) free space (air) and anything in between.

The utility of the approaches presented in this Thesis would truly be realized by integrating the constraint identification/mapping with the safe-manipulation algorithm. The target approach would be to use explored stiffness regions to make non-local trajectory optimization, by predicting the force, stiffness and elasticity many steps ahead of the local configuration.

While the approaches presented are blind, they could be enhanced with a-priori information. If the clustering classification algorithm is given a set of training data (previously obtained experimental data from similar environments), it could be used for haptic exploration and localization. The target application would be in searching for a constraint, which is known to exist in the workspace, but whose location in the workspace is unknown (such as searching for a tumor/cyst on an organ).

Blind, safe manipulation in flexible environments, used in tandem with real time constraint identification/mapping, will allow a robot to simultaneously explore, characterize, and manipulate an elastic system safely without a-priori knowledge. This approach, if developed further, could eventually enable safe semi-autonomous cooperative manipulation of RSAs in applications such as organ retraction and organ manipulation, during surgical procedures.

BIBLIOGRAPHY

1. Guthart, Gary S, and J Kenneth Salisbury. “The Intuitive TM Telesurgery System : Overview and Application.” In *IEEE International Conference on Robotics and Automation*, 2-5, 2000.

2. Ding, Jienan, Kai Xu, Roger Goldman, Peter Allen, Dennis Fowler, and Nabil Simaan. “Design , Simulation and Evaluation of Kinematic Alternatives for Insertable Robotic Effectors Platforms in Single Port Access Surgery.” In *IEEE International Conference on Robotics and Automation*, 2-7, 2010.

3. Abbott, D.J., Chris Becke, R.I. Rothstein, and W.J. Peine. “Design of an endoluminal NOTES robotic system.” In *Intelligent Robots and Systems, 2007. IROS 2007. IEEE/RSJ International Conference on*, 410–416. IEEE, 2007. http://ieeexplore.ieee.org/xpls/abs_all.jsp?arnumber=4399536.

4. Degani, Amir, Howie Choset, Brett Zubiate, Takeyoshi Ota, and Marco Zenati. “Highly articulated robotic probe for minimally invasive surgery.” In *IEEE International Conference on Robotics and Automation*, 3273-6, 2006. http://www.ncbi.nlm.nih.gov/pubmed/19163406.

5. Xiao, Jing. “Automatic Determination of Topological Contacts in the Presence of Sensing Uncertainties *.” In *IEEE International Conference on Robotics and Automation*, 65-70, 1993.

6. Xiao, J. “Automatic Generation of High-Level Contact State Space.” *The International Journal of Robotics Research* 20, no. 7 (July 1, 2001): 584-606. http://ijr.sagepub.com/cgi/doi/10.1177/02783640122067552.

7. Bruyninckx, Herman, and Joris De Schutter. “Kinematic Models of Rigid Body Interactions for Uncertainties.” In *IEEE International Conference on Robotics and Automation*, 1007-1012, 1993.

8. Kitagaki, K., T. Ogasawara, and T. Suehiro. “Contact state detection by force sensing for assembly tasks.” In *IEEE International Conference on Multisensor Fusion and Integration for Intelligent Systems*, 366-370. Ieee, 1994. http://ieeexplore.ieee.org/lpdocs/epic03/wrapper.htm?arnumber=398431.

9. Dupont, Pierre E, Timothy M Schulteis, and D Howe. “Experimental Identification of Kinematic Constraints.” In *IEEE International Conference on Robotics and Automation*, 2677-2682, 1997.

10. Debus, Thomas J., Pierre E. Dupont, and Robert D. Howe. “Contact State Estimation Using Multiple Model Estimation and Hidden Markov Models.” *The International Journal of Robotics Research* 23, no. 4 (April 1, 2004): 399-413. http://ijr.sagepub.com/cgi/doi/10.1177/0278364904042195.

11. Okamura, a. M. “Feature Detection for Haptic Exploration with Robotic Fingers.” *The International Journal of Robotics Research* 20, no. 12 (December 1, 2001): 925-938. http://ijr.sagepub.com/cgi/doi/10.1177/02783640122068191.

12. Okamura, A M, M L Turner, and M R Cutkoslcy. “- Haptic Exploration of Objects with Rolling and Sliding.” In *IEEE International Conference on Robotics and Automation*, 2485-2490, 1997.

13. Allen, P.K., and K.S. Roberts. “Haptic object recognition using a multi-fingered dextrous hand.” In *Proceedings, 1989 International Conference on Robotics and Automation*, 342-347. IEEE Comput. Soc. Press, 1989. http://ieeexplore.ieee.org/lpdocs/epic03/wrapper.htm?arnumber=100011.

14. Liu, Hongbin, Jichun Li, Xiaojing Song, Lakmal D Seneviratne, and Kaspar Althoefer. “Identification During Minimally Invasive Surgery.” In *IEEE transactions on robotics*, 27:450-460, 2011.

15. Xu, Kai, Student Member, and Nabil Simaan. “An Investigation of the Intrinsic Force Sensing Capabilities of Continuum Robots.” In *IEEE International Conference on Robotics and Automation*, 24:576-587, 2008.

16. Mehrandezh, M., and K.K. Gupta. “Simultaneous path planning and free space exploration with skin sensor.” In *Proceedings 2002 IEEE International Conference on Robotics and Automation (Cat. No.02CH37292)*, 4:3838-3843. Ieee, 2002. http://ieeexplore.ieee.org/lpdocs/epic03/wrapper.htm?arnumber=1014319.

17. Rodriguez, S., J.M. Lien, and N.M. Amato. “Planning motion in completely deformable environments.” In *Robotics and Automation, 2006. ICRA 2006. Proceedings 2006 IEEE International Conference on*, 2466–2471. IEEE, 2006. http://ieeexplore.ieee.org/xpls/abs_all.jsp?arnumber=1642072.

18. Patil, Sachin, and Ron Alterovitz. “Toward automated tissue retraction in robot-assisted surgery.” In *Robotics and Automation (ICRA), 2010 IEEE International Conference on*, 2088–2094. IEEE, 2010. http://ieeexplore.ieee.org/xpls/abs_all.jsp?arnumber=5509607.

19. Gayle, Russell, Paul Segars, MC Lin, and D. Manocha. “Path planning for deformable robots in complex environments.” In *Proc. of Robotics: Science and Systems (RSS)*, 225–232. Citeseer, 2005. http://citeseerx.ist.psu.edu/viewdoc/download?doi=10.1.1.104.1601&rep=rep1&type=pdf.

20. Huang, Shuguang, and J.M. Schimmels. “The bounds and realization of spatial stiffnesses achieved with simple springs connected in parallel.” In *Robotics and Automation, IEEE Transactions on*, 14:466–475. IEEE, 1998. http://ieeexplore.ieee.org/xpls/abs_all.jsp?arnumber=678455.

21. Roberts, R.G. “Minimal realization of a spatial stiffness matrix with simple springs connected in parallel.” In *Robotics and Automation, IEEE Transactions on*, 15:953–958. IEEE, 1999. http://ieeexplore.ieee.org/xpls/abs_all.jsp?arnumber=795799.

22. Roberts, R.G. “Minimal realization of an arbitrary spatial stiffness matrix with a parallel connection of simple and complex springs.” In *Robotics and Automation, IEEE Transactions on*, 16:603–608. IEEE, 2000. http://ieeexplore.ieee.org/xpls/abs_all.jsp?arnumber=880811.

23. Ciblak, Namik, and H. Lipkin. “Synthesis of Cartesian stiffness for robotic applications.” In *Robotics and Automation, 1999. Proceedings. 1999 IEEE International Conference on*, 3:2147–2152. IEEE, 1999. http://ieeexplore.ieee.org/xpls/abs_all.jsp?arnumber=770424.

24. Huang, Shuguang, and Joseph M Schimmels. “The Eigenscrew Decomposition of Spatial.” In *IEEE Transactions on Robotics and Automation*, 6:146-156, 2000.

25. McAllister, PL. “An eigenscrew analysis of mechanism compliance.” *Robotics and Automation, 2000.* (2000). http://ieeexplore.ieee.org/xpls/abs_all.jsp?arnumber=845173.

26. Lipkin, Harvey, and Timothy Patterson. “Generalized center of compliance and stiffness.” In *IEEE International Conference on Robotics and Automation*, 54:1161-1164, 1992. http://www.ncbi.nlm.nih.gov/pubmed/19962288.

27. Higham, NJ. “Computing a nearest symmetric positive semidefinite matrix.” *Linear algebra and its applications* 118 (1988). http://www.sciencedirect.com/science/article/pii/0024379588902236.

28. F. Fahimi *Autonomous Robots: Modeling, Path Planning* and Control, New York, NY, Springer Science + Business Media , 2009

29. J. Nocedal and S. J. Wright, *Numerical Optimization*, New York NY, Springer-Verlag (1999)

30. Poole, David L., and Alan K. Mackworth. *Artificial Intelligence: Foundations of Computational Agents*. New York, NY: Cambridge University PRess, 2010.

31. Korf, Richard E. “Real-time heuristic search.” *Artificial Intelligence* 42, no. 2-3 (March 1990): 189-211. http://linkinghub.elsevier.com/retrieve/pii/0004370290900544.

32. Griffis, Michael, and J. Duffy. “Comparing structures of stiffness matrices using invariants.” *RoManSy 9*, no. 3 (1993): 85–92. http://www.springerlink.com/index/M685515657663T85.pdf.

33. Ma, Burton, and R. Ellis. “Spatial-stiffness analysis of surface-based registration.” *Medical Image Computing and Computer-Assisted Intervention–*

MICCAI 2004, no. 1 (2004): 623–630. http://www.springerlink.com/index/HEYHPN967Q5TJFAE.pdf.

34. Yuan, JS. "Closed-loop manipulator control using quaternion feedback." *Robotics and Automation, IEEE Journal of* 4, no. 4 (1988): 434–440. http://ieeexplore.ieee.org/xpls/abs_all.jsp?arnumber=809.

35. A. Petrovskaya, O. Khatib, S. Thrun, and A. Y. Ng. "Bayesian estimation for autonomous object manipulation based on tactile sensors" *Proceedings of the 2006 IEEE International Conference on Robotics and Automation,* 2006

36. Goldman, R. E., Bajo, A. & Simaan, N (2011). Compliant Motion Control for Continuum Robots with Intrinsic Actuation Sensing. In *2011 IEEE International Conference on Robotics and Automation*, pages 1126-1132. Shanghai, China.

37. Goldman, R. (2011). *Analysis, Algorithms, and Control for Intelligent Surgical Exploration and Intervention*. Phd Thesis, Columbia University

38. Yamamoto, Tomonori, Balazs Vagvolgyi, Kamini Balaji, Louis L. Whitcomb, and Allison M. Okamura. "Tissue property estimation and graphical display for teleoperated robot-assisted surgery." *2009 IEEE International Conference on Robotics and Automation* (May 2009): 4239-4245. http://ieeexplore.ieee.org/lpdocs/epic03/wrapper.htm?arnumber=5152674.

39. Lin, Q., J.W. Burdick, and E. Rimon. "A stiffness-based quality measure for compliant grasps and fixtures." *IEEE Transactions on Robotics and Automation* 16, no. 6 (2000): 675-688. http://ieeexplore.ieee.org/lpdocs/epic03/wrapper.htm?arnumber=897779.

40. **Arora, J.S.**, *Introduction to Optimum Design*, Second Edition, Elsevier Academic Press, **2004**.

41. Rosen, Jacob, Jeffrey D Brown, Lily Chang, Mika N Sinanan, and Blake Hannaford. "Generalized approach for modeling minimally invasive surgery as a stochastic process using a discrete Markov model." In *IEEE transactions on bio-medical engineering*, 53:399-413, 2006. http://www.ncbi.nlm.nih.gov/pubmed/16532766.

42. Hart, John C., George K. Francis, and Louis H. Kauffman. "Visualizing quaternion rotation." *ACM Transactions on Graphics* 13, no. 3 (July 1, 1994): 256-276. http://portal.acm.org/citation.cfm?doid=195784.197480.

43. Kuipers, Jack. B. *Quaternions and Rotation Sequences*. 2nd ed. Princeton, NJ: Princeton University Press, 1999.

44. Lefebvre, Tine, Herman Bruyninckx, and J. De Schutter. "Polyhedral contact formation identification for autonomous compliant motion: Exact nonlinear

Bayesian filtering." *Robotics, IEEE Transactions on* 21, no. 1 (2005): 124–129.

45. Yamada, H. *Strength of Biological Material*, Baltimore, William&Wilkins (1970)
46. Y.C. Fung *Biomechanics: Mechanical Properties of Living Tissues*, New York, NY, Springer (1993)
47. Bajo, A., Goldman, R. E. & Simaan, N (2011). Configuration and Joint Feedback for Enhanced Performance of Multi-Segment Continuum Robots. In *2011 IEEE International Conference on Robotics and Automation*, pages 2905-2912. Shanghai,

VII Appendix A: Code

VII.A Simulation Code:

The following includes all the code in the red-triangle simulations used in section IV of the thesis.

VII.A.1 Simulation.m

Purpose: The main simulation file, starts the planar red triangle simulation

Associated files: sim2D.m

Notes: By itself, this code does little to nothing. It simply calls a set of functions, each of which perform a specific macro-task (such as calculating $\hat{\boldsymbol{p}}$, or graphing the simulation) from the general safe manipulation algorithm. These functions are methods in the sim2D class, which takes care of all the "under the hood" specific code.

```
clear
close all
clc
%Define Starting and goal configurations

start = [63.3013,  36.5470, 0, 0, 0, pi/2]';
goal = [100, 100, 0, 0, 0, 1.6]';

%Create a simulation object
PP = sim2D(start, goal);

%Set Path Planner Parameters
PP.alpha = [1/20; .001; 20;  5];
PP.controller = [.3, -.3, .05];

%Misc. variables
df = 10; %Discretization factor
```

```
t = 1;

while PP.convergence == 0


    %% Evaluate Tasks and Constraints at current configuration
    %-------------------------------------
    constr = PP.EvaluateConstraint(1);

    if PP.constraint > 0
        PP.RedFlag;
        PP.backtrack;
    end

    task = PP.EvaluateTask(1);

    if task < PP.eps
        PP.convergence = 1;
        break
    end

    %-------------------------------------


   %% Evaluate motion direction

 % Update the node directions every df steps
 if (floor(PP.k/df) == PP.k/df || PP.k == 1)

 % Markov Model Behavior selection

PP.markov_update;

%Behavior Selection
    switch PP.markov_state


        case 3 %Backtracking
            p  = PP.dim_weight*(PP.safe_points(:,PP.z-1) - PP.cnfg);
            p = p/norm(p);
            PP.backtrack;

        case 2   %Random Walk

            p = zeros(6,1);

            p(1) = rand-.5;
            p(2) = rand-.5;
            p(6) = (rand-.5)*PP.alpha(1);

            p = p/norm(p);

            PP.GenerateSafePoint
```

```
        case 1  %Normal State

             p = PP.deriv;

             PP.GenerateSafePoint

    end


  %% Calculate control velocity

      %Calculate movement from current configuration
    %-----------------------------------------------
    kd = PP.controller(1);
    kv = PP.controller(2);
    ki = PP.controller(3);

    v = PP.v;
    d = PP.distance;


    v = kd*d + ki*PP.intd + kv*v;
    v = v*1/(norm(constr))^.3;

    if v > 10
        v = 10;
    end

    PP.v = v;
    %-----------------------------------------------

end

  %% Update, Increment Simulation

    %Graphical output of current configuration
    PP.graphsim;

        %Increment simulation
    %-------------------------------------------------------
            %Calculate the steepest descent direction


            %Calculate the next movement step
            PP.cnfg = PP.cnfg + PP.v*PP.dt*p;

            %Integrate the distance, d
            d = PP.distance;
            PP.intd = PP.intd + d*PP.dt;

            M(PP.k) = getframe(1);
```

```
            %Increment the simulation counter
            PP.k = PP.k + 1;

    %-----------------------------------------------------

  end
```

VII.A.2 Sim2D.m

Purpose: Contains all the data, under-the-hood functions necessary to run the red triangle simulation

Associated files: sim2D.m

Notes: Don't read this file first. Each of the functions in Sim2D is specifically referring to some point in the simulation.m code.

```
  classdef sim2D < handle
      % Creates a sim2D object, which is a simulation of a planar robot
being
      %manipulated within a flexible environment.

      % All the parameter data is stored in the object properties, and
can be
      % called upon by the class methods

      % The sim2D object replaces the individual simulation .m files
used in
      % previous versions


      properties (SetAccess=protected)

          %The following set of properties fully define the unknown
          %parameters of the elastic environment in which the 2d object
is
          %being manipulated

          %Defines position of the ground links in 3 dimensional
vectors
```

```
            Links = [63.3013, 109.6410, 0;
                      0,          0,    0;
                     126.6026,    0,    0]';

            %Defines the spring constant and free length of the springs
            kc =[1.39; 1.39; 1.39];
            lo =[50; 50; 50];
        end



        properties (SetAccess= public)

            %These define the starting and ending configurations for the
robot
            cnfg = [0; 0; 0; 0; 0; 0];
            goal   = [10; 10; 0; 0; 0; .5];

            %This defines the geometry of the robot
            robot =  23.02*[ cosd(0),  sind(0),   0;
                        cosd(120), sind(120), 0;
                        cosd(240), sind(240), 0]';

            %A list of the different safe points and red flags currently
stored
            %within the simulation
            safe_points = zeros(6,1);
            red_flags   = zeros(6,1);


            %The dimensional weighting scheme
            dim_weight = diag([1; 1; 0; 0; 0; 1/23]);


            %Controller and task/constraint law parameters,
            %which determine the scaling of the potential field and the
            %behavior of the motion planner PID controller, respectively
            controller = [1.6 -1 1];
            alpha = [0, 0, 0, 0];

            %General Simulation variables
            dt          = .05;    %Time step
            eps         = .1;   %Convergence tolerance
            k = 1;                %Simulation step counter

            constraint = 0;       %Binary constraint value, representing
            convergence = 0;                        % 'has a constraint been
violated yet?'


            %History variables, storing relevent force and position
            %to memory
            xi_hist = [0, 0, 0, 0, 0, 0];
            We_hist = [0, 0, 0, 0, 0, 0];
```

```
            K_hist = zeros(6,6,1);

            %Misc. variables
            intd = 0;
            v = 0;
            z = 0;
            y = 0;
            markov_state = 1;

        end

        methods

            function PP = sim2D(start, goal)
                PP.cnfg = start;
                PP.goal = goal;
            end

            function setspringparam(PP,Links, kc, lo)
                PP.Links = Links;
                PP.kc = kc;
                PP.lo = lo;
            end


            function We = Force_Measurement(PP)

                % ----------------- Position of Robot -------------------
------
                xi = PP.cnfg;
                % Defines Rotation matrices based on the euler angles
specified in th =[thx, thy, thz]'
                        Rx = [1        0             0;
                              0 cos(xi(4)) -sin(xi(4));
                              0 sin(xi(4))  cos(xi(4))];

                        Ry = [cos(xi(5)) 0  sin(xi(5));
                              0          1           0;
                             -sin(xi(5)) 0  cos(xi(5))];


                        Rz = [cos(xi(6)) -sin(xi(6)) 0;
                              sin(xi(6)) cos(xi(6))  0;
                              0           0          1];

                %Rotate about x,y, then z world frame axes
                   R = Rz*Ry*Rx;

                %Orients the triangle w.r.t. the world frame based on
input euler angles
                 bi = R*PP.robot;

               %Defines the vertices of the triangles
```

```
            xii = [bi(:,1) + xi(1:3,1), bi(:,2) + xi(1:3, 1), bi(:,3)
+ xi(1:3, 1)];

            %The length vector for each spring
            li = xii - PP.Links;

            %The normalized length vector for each spring
            si = [li(:,1)/norm(li(:,1)), li(:,2)/norm(li(:,2)), li(:,
3)/norm(li(:, 3))];


            %--------------------- Force Calculation ----------------
--------

            %Defines Jacobian and Force Vectors
            Jp = [si(:, 1)               , si(:, 2)                ,
si(:, 3)               ;
                cross(bi(:,1),si(:,1)),       cross(bi(:,2),si(:,2)),
cross(bi(:,3), si(:,3))];



            %Calculate tau vector (Spring forces)
            tau = [PP.kc(1)*(norm(li(:,1)) - PP.lo(1));
                   PP.kc(2)*(norm(li(:,2)) - PP.lo(2));
                   PP.kc(3)*(norm(li(:,3)) - PP.lo(3))];


            %Calculates the reaction spring wrench
            We = -Jp*tau;
        end

        function  constraint = EvaluateConstraint(PP, i)

            %Evaluates the Constraint function based on the desired
input
            %constraint law. If i == 1, then the first set of rules
is used
            %to define the constraint function, and if i== 2, the
second
            %set of rules is used, etc...

            if i ==1

            % Conservative force constraint
            %--------------------------------------
            We = Force_Measurement(PP);
            We(6,1) = 0;
            F = norm(PP.dim_weight*We);

             Fcrit = 50; %N
            constraint_1 = PP.alpha(3)/(Fcrit - F);
            %----------------------------------------
```

```
            % Avoid Red flags constraint
            %--------------------------------

            % If there are any red flags
            if PP.y > 0
            dist_to_flag(1:PP.y,1) = inf;
            constraint_2 = 0;


            for j = 1:PP.y
                %Calculate    the    distance    from    the    current
configuration to
                %Each red flag configuration
                dist_to_flag(j,1)   =   norm(PP.dim_weight*(PP.cnfg   -
PP.red_flags(:,j)));
                %Add the potential field for each red flag

                % Add exception for negligiable distances
                if dist_to_flag(j,1) < .01
                constraint_2 = constraint_2 + 10;
                else
                constraint_2   =   PP.alpha(4)/dist_to_flag(j,1)^.4   +
constraint_2;
                end
            end

            constraint_2 = constraint_2*PP.EvaluateTask(1);
            % If no red flags, no constraint

            else

                constraint_2 = 0;

            end

            %-------------------------------------------------------
-----
            %Constraint Law
            constraint = constraint_1 + constraint_2;

            %Defining the binary constraint
            PP.constraint = (F>Fcrit);

            else
                constraint = 0;
            end
        end

        function task = EvaluateTask(PP, i)

            %Evaluates the task function, which defines the set of
            %attractive potential fields centered about the goal.
```

```
            if i==1
                dv = (PP.dim_weight)*(PP.goal - PP.cnfg);
                d = norm(dv);
                task = .5*d^2;
            end
        end


        function J = J(PP)

            %The function J simply adds the Task function on top of
the
            %Constraitn function, to construct the total artificial
            %potential field

        J = EvaluateTask(PP,1)+ EvaluateConstraint(PP,1);

        end



        function [p, dJ_dx, K] = deriv(PP)

            %The following function performs a simple routine which
            %perturbs the robot along each dimension of the
configuration,
            %in order to evaluate the derivative of the artificial
            %potential field.

            dJ_dx = zeros(6,1);
            p = dJ_dx;


            J_current = J(PP);
            We_current = Force_Measurement(PP);


            for i = 1:6
            %Move along each dimension of xi
            dxi = zeros(6,1);
            delta = .1;

            %Adjust for angular displacements
            b = norm(PP.robot(:,1));
            if i > 3
                delta = delta/b;
            end

            dxi(i,1) = delta;


            PP.cnfg = PP.cnfg + dxi;
```

```
            dJ_dx(i,1) = (J(PP) - J_current)/delta;
            We = Force_Measurement(PP);

            K(:,i) = (We - We_current)/delta;

            PP.cnfg = PP.cnfg - dxi;
            end

            dJ_dx = PP.dim_weight*dJ_dx;

            p = -dJ_dx/norm(dJ_dx);
        end

        function v = Position_Controller(PP)

            kd = PP.controller(1);
            kv = PP.controller(2);
            ki = PP.controller(3);
            d = PP.distance(PP);
            v = PP.v;

            v = kd*d + ki*PP.intd + kv*v;
            PP.v = v;

        end

        function d = distance(PP)
            d = norm(PP.dim_weight*(PP.goal-PP.cnfg));
        end



        function graphsim(PP)

          % Graphing function graphs out the environment, triangles,
etc..

          % ----------------- Position of Robot ---------------------
----
            xi = PP.cnfg;

            % Defines Rotation matrices based on the euler angles
specified in th =[thx, thy, thz]'
                    Rx = [1        0             0;
                          0 cos(xi(4)) -sin(xi(4));
                          0 sin(xi(4))  cos(xi(4))];

                    Ry = [cos(xi(5)) 0  sin(xi(5));
                          0          1           0;
                         -sin(xi(5)) 0  cos(xi(5))];


                    Rz = [cos(xi(6)) -sin(xi(6)) 0;
```

```
                        sin(xi(6)) cos(xi(6))  0;
                        0           0          1];

            %Rotate about x,y, then z world frame axes
               R = Rz*Ry*Rx;

            %Orients the triangle w.r.t. the world frame based on
input euler angles
             bi = R*PP.robot;

            %Defines the vertices of the triangles
             xii = [bi(:,1) + xi(1:3,1), bi(:,2) + xi(1:3, 1), bi(:,3)
+ xi(1:3, 1)];


            %-----------------------------------------------------------
------


            % Defines Rotation matrices based on the euler angles
specified in th =[thx, thy, thz]'
                    Rx = [1        0             0;
                          0 cos(PP.goal(4)) -sin(PP.goal(4));
                          0 sin(PP.goal(4))  cos(PP.goal(4))];

                    Ry = [cos(PP.goal(5)) 0  sin(PP.goal(5));
                          0          1           0;
                         -sin(PP.goal(5)) 0  cos(PP.goal(5))];


                    Rz = [cos(PP.goal(6)) -sin(PP.goal(6)) 0;
                          sin(PP.goal(6)) cos(PP.goal(6))  0;
                          0           0          1];

            %Rotate about x,y, then z world frame axes
               R = Rz*Ry*Rx;

            %Orients the triangle w.r.t. the world frame based on
input euler angles
             bi_goal = R*PP.robot;

            %Defines the vertices of the triangles
             xii_goal = [bi_goal(:,1) + PP.goal(1:3,1), bi_goal(:,2) +
PP.goal(1:3, 1), bi_goal(:,3) + PP.goal(1:3, 1)];


             figure(1)
             hold off
             plot(0, 0)

             hold all
             plot([xii(1,:) xii(1,1)],[xii(2, :) xii(2,1)], 'r-*')
             plot([xii_goal(1,:)     xii_goal(1,1)],[xii_goal(2,     :)
xii_goal(2,1)], 'b-*')
```

```
            plot(PP.Links(1, :),PP.Links(2, :), 'sb')

            axis equal
            plot([PP.Links(1,1)  xii(1,1)],[PP.Links(2,1)  xii(2,  1)],
'g')
            plot([PP.Links(1,2)  xii(1,2)],[PP.Links(2,2)  xii(2,  2)],
'g')
            plot([PP.Links(1,3)  xii(1,3)],[PP.Links(2,3)  xii(2,  3)],
'g')
            xlabel('mm')
            ylabel('mm')


            % Plot Safe Points

            plot(PP.safe_points(1,:), PP.safe_points(2,:), 'b-*');

            % Plot Red flags
                if PP.y > 0
                plot(PP.red_flags(1, :), PP.red_flags(2, :), 'r*');
                end

        end


        function GenerateSafePoint(PP)

            %This function plots a new point along the trajectory

             PP.z = PP.z+1;  %Increment the safe point count
             PP.safe_points(:,PP.z) = PP.cnfg; % Add current config
as a safe point

        end



        function backtrack(PP)
           % This function effectively performs backtracking to the
           % previous node


           % Brute force move to previous node
            PP.cnfg = PP.safe_points(:, PP.z);


           % Delete the last safe point, unless there is only one
safe
           % point
            if ~(PP.z == 1);
            PP.safe_points(:,PP.z) = [];     % Eliminate from stored
values
            PP.z = PP.z-1;                % Decrement counter
```

```
    end
end



function RedFlag(PP)
%Define red flags counter


% Do not plant a red flag while backtracking
if ~(PP.markov_state == 3)

% If no red flags
if PP.y == 0

 % Define initial red flag
PP.y = PP.y+1;
PP.red_flags(:,PP.y) = PP.cnfg;

else

 % Otherwise, see if any nearby red flags
 %=========================================
 dist_to_red_flags = zeros(PP.y, 1);


for j=1:PP.y
    dist_to_red_flags(j,1)    =    norm(PP.dim_weight*(PP.cnfg-
PP.red_flags(:,j)));
end


[dist, point_number] = min(dist_to_red_flags);
%=======================================================

% if no red flags within 4 units of current config, define
new red
% flag
if (dist > 4)
PP.y = PP.y+1;
PP.red_flags(:,PP.y) = PP.cnfg;
end

    end

end

% Set markov state to Backtrack
PP.markov_state = 3;

end

function K = stiffness(PP, xi)
```

```
            xi_old = PP.cnfg;
            PP.cnfg = xi;
            [p, J, K] = PP.deriv;
            PP.cnfg = xi_old;
        end


        function new_state = markov_update(PP)

            %Purpose of the function is to update the Markov Chain in
the
            %sytem

            %Obtain the current state of the system
            current_state = PP.markov_state;

            %Obtain random number, to decide new state
                    p = rand;


            %Assign  new  state  based  on  the  current  state,  random
number
            switch current_state

                % Normal state
                %-------------------------
                case 1
  %                    disp(num2str(p))
                    % 90% chance of staying in normal state
                    if p < .9

                        new_state = 1;

                    else % 10% chance of moving to random sate
                        disp('random state')
                        new_state = 2;

                    end


              % Random State
              %---------------------------

                case 2

                    % 60% chance of staying in random state
                     if p < .6

                         new_state = 2;

                     else % 40 % chance of normal state

                         new_state = 1;
```

```
                end

            %Backtracking State
            %-----------------------------------
             case 3


                % 60% chance of staying in backtracking state

                if p < .6

                    new_state = 3;


                else               % 10% chance of random state

                    new_state = 1;

                end

            end

            PP.markov_state = new_state;

        end

    end

end
```

VII.B Robot Control Code

Overview:

The Puma560 robot control code, shown below in figure A.1, involves 3 primary subsystems:

- **Puma560**
  - Sends motor control signals to actual Puma560 robot (via control/Daq cards)
  - Recieves potentiometer and encoder readings from Puma motors
    - Calculates Robot's joint angles
- **PD + Inverse Dynamics**
  - Uses computed torque to compensate for robot dynamics
  - PD controller for joint-level position control
- **Trajectory planner**
  - Determines desired trajectory in joint space
    - Joint positions, velocities, accelerations
  - Has multiple modes, including cartesian control and position control

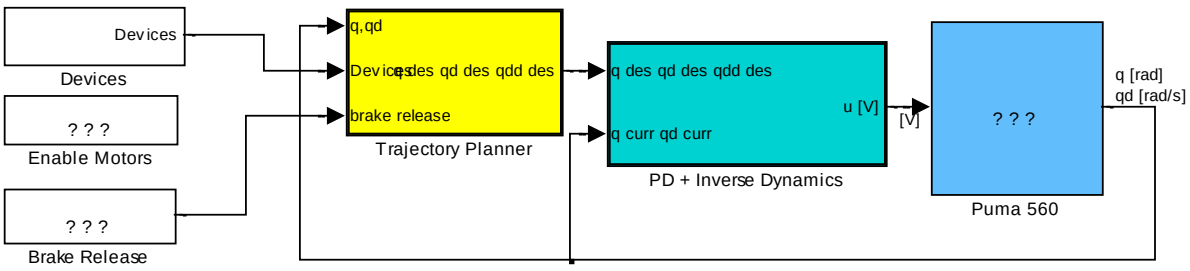

Figure A.1 Puma560 main control code

VII.B.1 Non-Application-Specific code

Below is a set of Simulink blocks/subsystems which are not specific to the applications presented in this thesis, but are rather for general kinematic control of the robot.

PD + Inverse Dynamics:

This code was written by lab member Andrea Bajo, in 2009

Figure A.2 is a diagram of the PD + Inverse dynamics block. It has 3 general components

- Determining the appropriate control signal
- Determining the system dynamics
- Converting control signal to voltage

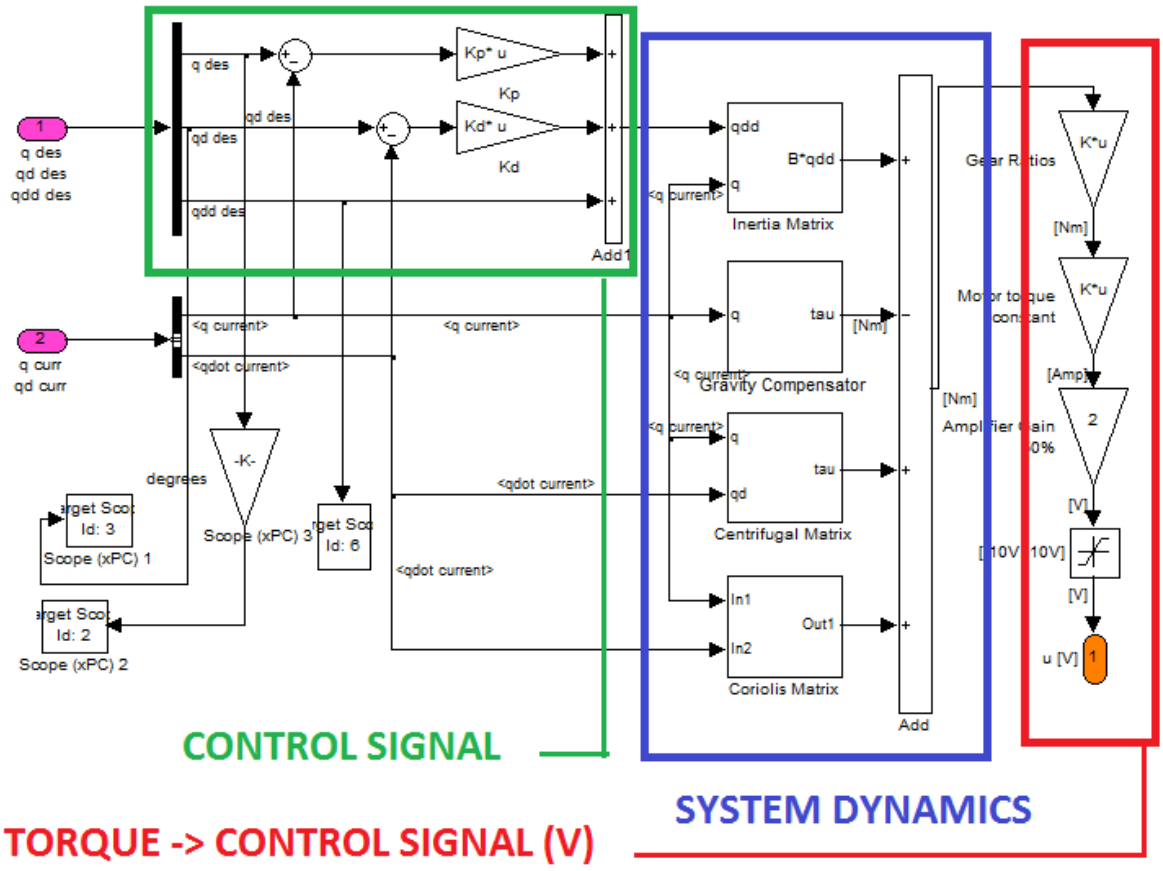

Figure A.2: PD+ Inverse dynamic block of the Puma 560 control code

Puma560 block

This code was also written by Andrea Bajo in 2009. Figure A.3 below is the Puma560 block, which interfaces with the actual robot. It can be broken down into 3 sections:

- Motor signals to robot
- Joint signals from robot
- Processing Joint signals

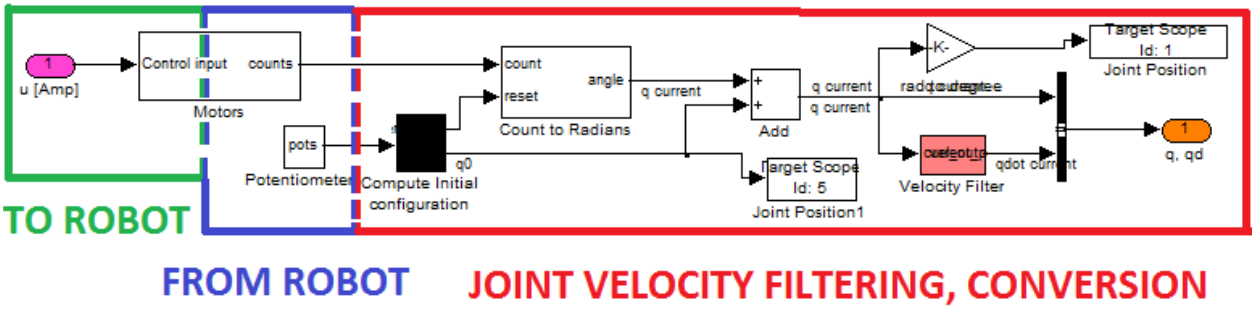

Figure A.3: Puma560 Interface subsystem

Trajectory Planner Block

The trajectory planner block switches the Puma between several different control modes (Cartesian control, Joint Space control, etc..). The code was designed by Sam Bhattacharyya in 2011, with some original sets of code in the first two subsystems written by Andrea Bajo and Francesco Senni. The last subsystem, Mode 4, contains all code used to implement the algorithms presented in the thesis.

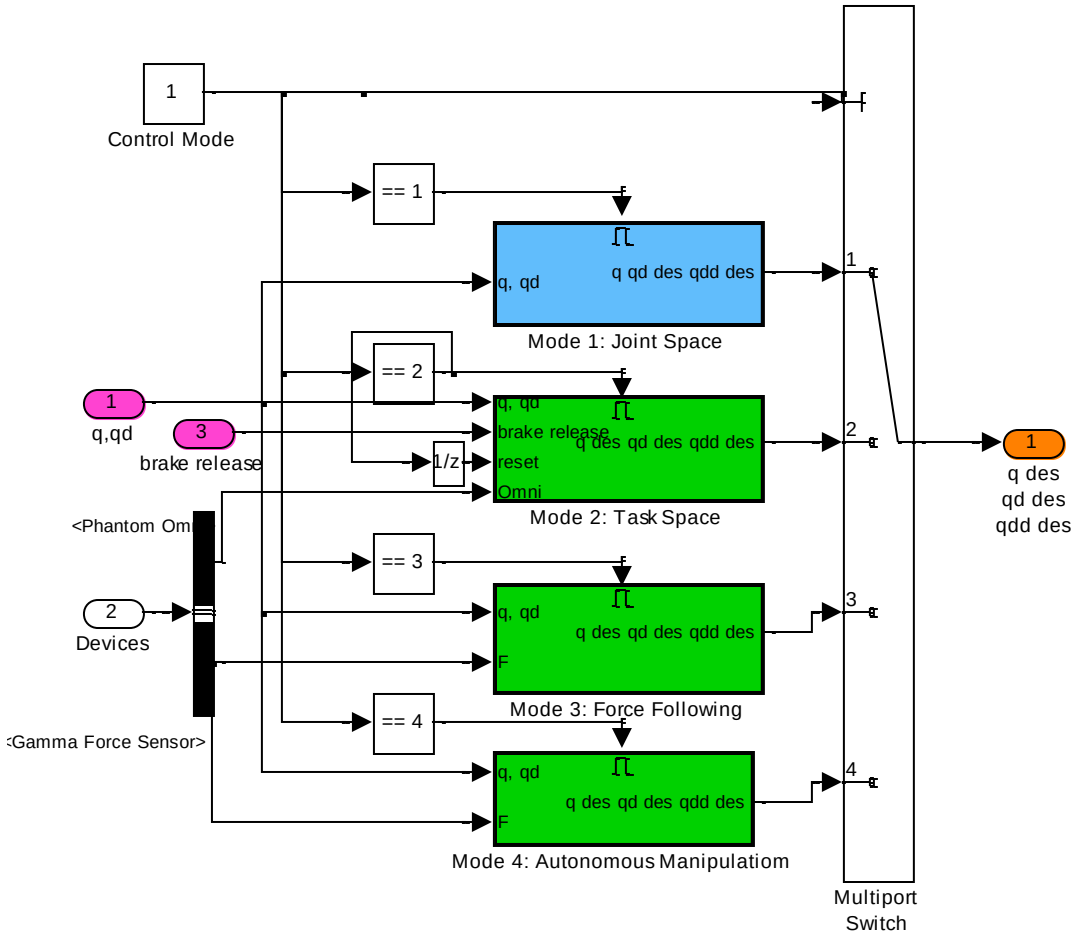

Figure A.4: Puma trajectory planner

VII.B.2 Application specific code

Autonomous manipulation section

In the Mode 4 subsystem, there are 3 main components. The first calculates the states $\zeta, \boldsymbol{w}_e$ from the force sensor, joint positions. The middle section is the Path Planner, and it directly implements the autonomous manipulation algorithm, as discussed in this thesis. It takes in the system states $\zeta, \boldsymbol{w}_e$, and outputs a task-space twist ξ. The final section converts the task space twist into a desired joint position, velocity and acceleration.

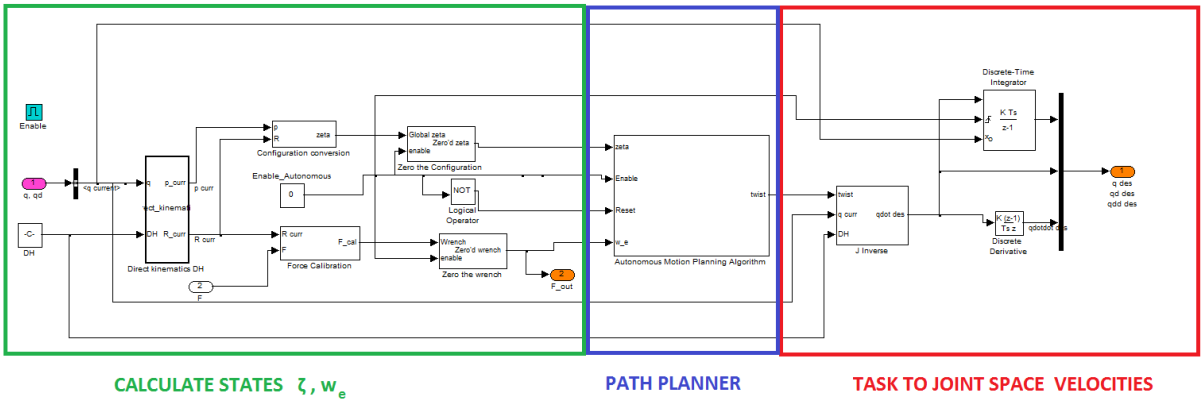

Figure A.5: Puma Path Planner

Path Planner

The Path Planner is the primary subsystem, which implements the algorithms/featured discussed in the autonomous navigation/stiffness exploration sections of this thesis.

At first glance, it looks complex, however it can be broken down very easily.

- The Path planner block acts as a hub for 5 subsystems, each of which represent a mode of operation
    - In the same way that the Trajectory planner is a hub for 4 control modes
- These subsystems reside within a switch, which is controlled by the behavior selector block (decides which subsystem should be enabled at the current time step)
- The subsystems are activated in a specific sequence: 1, 2, 3 and finally 4. Subsystem 5 is only activated under special circumstances.
- These subsystems all output a desired end effector twist
    - Default State
        - As soon as the robot switches to Mode 4: autonomous manipulation, the Default state is enabled

- The default state simply output's a desired manipulator twist of **0**, keeping the robot stationary

- Initialization State
  - This state simple perturbs the robot along each dimension, and measures the changes in end effector wrench (to calculate the initial K)
- Autonomous navigation
  - Performs the actual path planning code
  - Is similar to the planar path planning code
- Telemanipulation state
  - After the robot achieves a given manipulation goal, it switches to the telemenipulation state, which is also a
  -

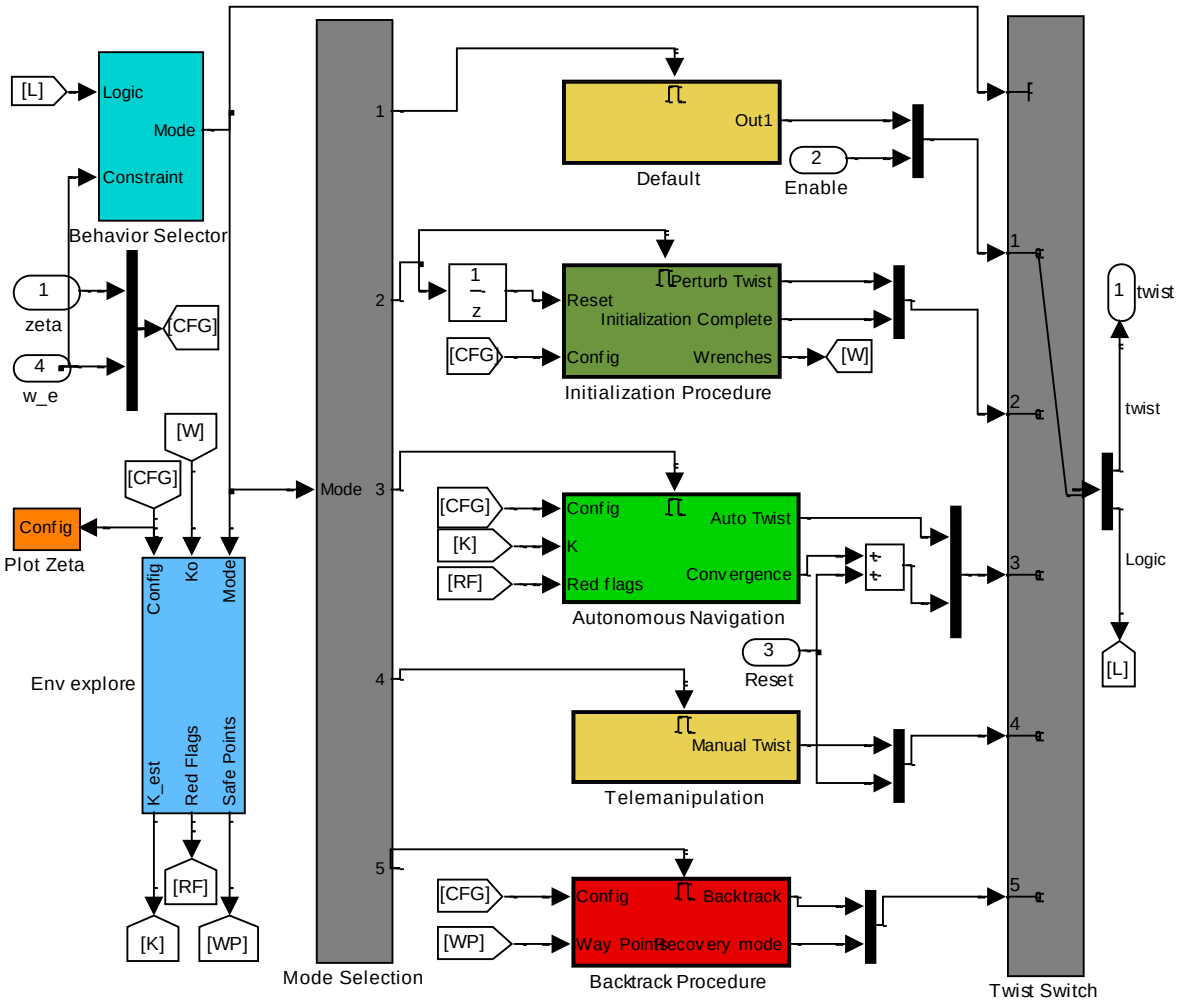

Figure A.6: Autonomous navigation Path Planner

Environmental Exploration:

Designed to run concurrentely with the regular code, it had 3 very simple subsystems:

- Way points
  - Stores the path history, termed here "way points", as a set of nodes in 7-dimensional space.
- Update K
  - Takes care of the K-updates, using the BFGS algorithm presented in this thesis
- Eigenscrew System
  - Does the eigenscrew decomposition to identify principle axes

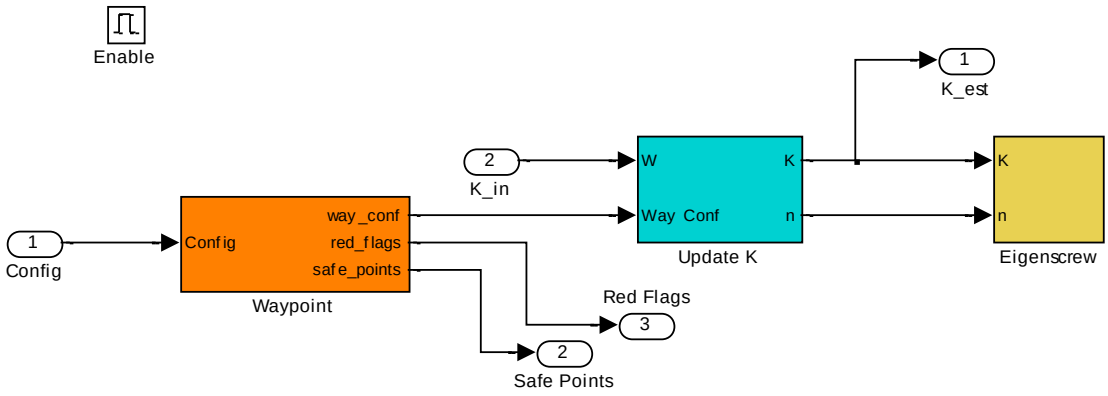

Autonmous navigation code

The following code is the core of the path planning algorithm, and is similar to the code used in the planar robot simulation. It takes in the current pose, wrench, K and set of red flags, and determines the output twist. The code to do shown below:

```
  function [p, e,  convergence, task_curr, constraint_curr] = fcn(zeta,
w_e, K, zeta_goal, w_cr)
  %#eml
```

```
% Define Initial Constants
%----------------------------------------
alpha = .043;

Gamma = diag([1, 1, 0, 0, 0, 0, alpha]);

% Dimensionality weighting matrix
% First three entries are in cartesian coord
% Last three entries are angular perturbations
Gamma_six = diag([1, 1, 1, 5, 5, 5]);

%The curent
eps = .005^2;

% 5mm = theoretical perturbation
delta = .02;
%----------------------------------------------------


%Calculate the current J value
J_curr = task(zeta, zeta_goal, Gamma) + constraint(w_e, w_cr,
Gamma_six, 0);
% J_curr = task(zeta, zeta_goal, Gamma);


task_curr = task(zeta, zeta_goal, Gamma);
constraint_curr = constraint(w_e, w_cr, Gamma_six, 0);

if task_curr < eps
    convergence = 1;
else

    convergence = 0;
end


dJ_dx = zeros(6,1);


for i = [1, 2, 6]


%Calculate the hypothetical next move
%-----------------------------------------
dxi = zeros(6,1);
dxi(i,1) =  delta;
dxi = (Gamma_six)*dxi;



%Calculate the change in each property
%-----------------------------------------------
dw_e = K*dxi;   %Calculate change in wrench
```

```
   dE = w_e.'*dxi;  %Calculate change in elastic energy
   dzeta = proppose(zeta, dxi); %Calculate the change in pose


   %Calclate the gradient
   dJ_dx(i,1) = (task(dzeta, zeta_goal, Gamma) + constraint(w_e + dw_e,
w_cr, Gamma_six, dE) - J_curr)/norm(dxi);
   % dJ_dx(i,1) = (task(dzeta, zeta_goal, Gamma) - J_curr)/norm(dxi);
   end


   p = -dJ_dx/norm(dJ_dx);

   p(4:6,1) = p(4:6,1);


   e = distance(zeta, zeta_goal, Gamma);









   end




   function task = task(zeta, zeta_goal, Gamma)

   d = distance(zeta, zeta_goal, Gamma);


   task = 1/2*d^2;



   end


       function d = distance(zeta, zeta_goal, Gamma)


          dr = zeta_goal(1:3, 1) - zeta(1:3, 1);

          dq = qmult(zeta_goal(4:7).', qinv(zeta(4:7).')).';

          dzeta = [dr; dq];
```

```
        d = sqrt(dzeta.'*Gamma*dzeta);
        d = norm(d - .014);


    end


function constraint  = constraint(w_e, w_cr, Gamma_six, E)

    %Radius of influence
    roi = .25; %m

    %Calculated weighted wrench
    w_weighted = sqrt(norm((Gamma_six*w_e)));

    %Calculate the correct wrench
    if w_cr < w_weighted
        constraint = 10^6;
    else
        constraint = abs(roi/(w_cr - w_weighted));
    end

    constraint = constraint + .1*E/w_cr;

end


function dzeta = proppose(zeta, dxi)
%The purpose of this function is to propogate the pose, based on the
input infinitessimal displacement given by dxi

%Calculate the angle of displacement
th = norm(dxi(4:6,1));

if th == 0
    dq = [1, 0, 0, 0];

else
    % Rotational axis
    o = (dxi(4:6).')/th;

    %Displacement quaternion
    dq = [cos(th/2), o*sin(th/2)];

end

% Current quaternion
qcurr = zeta(4:7)';

% Propogate the current quaternion, by rotation in world frame
qprop = qmult(dq, qcurr);
```

```
rprop = zeta(1:3) + dxi(1:3);

dzeta = [rprop; qprop.'];


end
```

VII.C Stiffness Code

VII.C.1 Process_K.m

Purpose: The point of this code was to calculate the SPSD approximates of K, and to then calculate the constraint vectors from those SPSD approximates, using a set of raw stiffness matrices K. Each K matrix was saved in a different .mat file, obtained directly from control code.

Associated files: A set of .mat files, no other code needed to function

```
for i = 1:15


% Load the .mat files
load(['Foam_' num2str(i) '.mat'])



% SPSD Approximate
%----------------
K_i = (-W)*T^-1;

B = (K_i + K_i.')/2;

[Z, L] = eig(B);

H = Z*L*Z.';
```

```
K = (B+H)/2;
%------------------


% Principle Axis Decomposition
%---------------------------
A  = K(1:3, 1:3);

B = K(1:3, 4:6);

D = K(4:6, 4:6);

Kv = A;

Kw = D - B.'*A^-1*B;
%-------------------------


% Eigenvalues
%----------------------
d =  abs(eig(Kv));

d = sort(d, 'descend');

r = abs(eig(Kw));
r = sort(r, 'descend');

%Tranlational
Tr(:, i) = d';

%Rotational
Ro(:, i) = r';
%---------------------------
end
```

VII.C.2 Particle Filter.m

Purpose: To estimate the optimal classification for a set of constraint vectors

Associated files: clusterfy.m, CU.m

```
%  Particle Filter
```

```
  %   The purpose of to classify constraint vectors using clustering,
which is
  %  optimized via particle filtering

  clear
  close all
  clc

  % Load the data
  load signatures
  load Locations


  % Number of classes
  k = 2;

  % Number of examples
  E = 15;

  % Particle Filter sample size
  n = 100;

  %  Classification  matrix,  each  row  is  the  classification  for  a
particle
  classification  = zeros(n, E);

  % Utility vector corresponding to each particle
  utility = zeros(n,1);


  % Load all examples into static variable
  e = Tr;   % Tr from signatures file

  % Number of Filters
  REP = 10;


  % Initial random classification
  %-----------------------------------------------------------

  for i = 1:n

      % Generate a set of random classification

      for j = 1:E
          %For each example, assign a random class
          classification(i,j) = ceil(rand*k);
      end
  end

  %-----------------------------------------------------------------
```

```
for reps = 1:REP


    for i = 1:n

    % Locally optimize each classification

    [classification(i,:)] = clusterfy(classification(i,:), e);


    utility(i,1) = CU(classification(i,:), e);
%       % Evaluate the utility of each classification
%       utility(i,1) = CU(classification(i,:), e);


    end

     %Randomized elimination
     %================================================

      norm_factor = max(utility(:,1));

      % Probability of elimination
      pdf = utility(:,1)/norm_factor;

      % Elimination vector
      elimination_vector = zeros(n,1);

      for i = 1:n

          p = rand;

          if pdf(i,1) > p

              elimination_vector(i,1) = 1;

          end

      end

      % Replace eliminated variables with new random classifications

      for i = 1:n

          if elimination_vector(i,1)

          for j = 1:E
        %For each example, assign a random class
        classification(i,j) = ceil(rand*k);
          end
```

```
            end
        end


    end



    % Graph the results
    figure(1)
    hold on


    for j = 1:15
    % Graph each node


    % Decide the color based on it's class
    %-----------------------------------------
        clss = optimal(1, j);

        switch  clss

            case 1
            clr = 'b';

            case 2

             clr = 'r';
        end
    %-----------------------------------------

    % Plot
        spcs = [clr 'o'];
        plot3(e(1,j), e(2,j), e(3,j), spcs, 'MarkerSize', 5, 'LineWidth',
4);
    end

    grid on
```

VII.C.3 clusterfy.m

Purpose: To locally optimize a set of clusters, designed to be operated with a particle filter, with a set of classifications (particles).

Associated files: Particle_Filter.m

```
  function [classifications, utility] = clusterfy(classification,
examples )
  %UNTITLED2 Summary of this function goes here
  %   Detailed explanation goes here



  % Number of examples
  E = length(classification(1,:));



  % Number of particles
  n = length(classification(:, 1));

  sse = zeros(n, E);

  utility = zeros(n,1);


  % For each particle
  for i = 1:n



  % Number of classes
  k = max(max(classification(i,:)));

  % Class count variable
  clss_cnt = zeros(k,1);

  % Average value of each class
  clss_av = zeros(3, k);

  % k lists, one for each class
  classes = zeros(k, 15);


  reor = zeros(k,1);
```

```
    % Locally optimize each particle
    for t = 1:1



%  First, populate the class lists
%---------------------------------

        for j = 1:E

        clss = classification(i, j);

        clss_cnt(clss) = clss_cnt(clss) + 1;

        classes(clss, clss_cnt(clss)) = j;

        end
%-------------------------------------

% Find the class average
%----------------------------------------
    for clss = 1:k

        %Clear the class average
        clss_av(:,clss) = 0;

        for j = 1:clss_cnt(clss)

        % the current node n, in class i
        node = classes(clss, j);

        %Class average
        clss_av(:,clss) = clss_av(:,clss) + examples(1:3, node);

        end

        clss_av(:, clss) = clss_av(:, clss)/clss_cnt(clss);

    end

 %-----------------------------------------


   % Assign each node to new class
%-------------------------------------

    for j = 1:15


 %For the current node
```

```
     %Find best fit, for node to class
     %-------------------------------
        for clss = 1:k

        v = examples(1:3, j) - clss_av(:,clss);

        reor(clss) = v.'*v;

        end


        [y, clss] = min(reor);

    %-------------------------------------


    %Re-assign node to class

       classification(i,j) = clss;


       end


       % Examples improved one step for one particle

       end

       % Examples improved all steps (locally optimized), for one
particle


   end

       % Examples locally optimized, for all particles



       classifications = classification;



   end
```

VII.C.4 CU.m

Purpose: To calculate the fitness function for a particular classification of a set of examples

Associated files: Particle_Filter.m

```
function [utility] = CU(classification, examples )




% Number of examples
E = length(classification(1,:));



% Number of classes
k = max(max(classification(1,:)));


% Class count variable
clss_cnt = zeros(k,1);

% Average value of each class
clss_av = zeros(3, k);

% k lists, one for each class
classes = zeros(k, 15);

%  First, populate the class lists
%-----------------------------------

        for j = 1:E

        clss = classification(1, j);
```

```
        clss_cnt(clss) = clss_cnt(clss) + 1;

        classes(clss, clss_cnt(clss)) = j;

        end
%-------------------------------------

% Find the class average
%----------------------------------------
    for clss = 1:k

        %Clear the class average
        clss_av(:,clss) = 0;

        for j = 1:clss_cnt(clss)

        % the current node n, in class i
        node = classes(clss, j);

        %Class average
        clss_av(:,clss) = clss_av(:,clss) + examples(1:3, node);

        end

        clss_av(:, clss) = clss_av(:, clss)/clss_cnt(clss);

    end
    %-----------------------------------------



    % Find the sum of squared error
    %--------------------------------------

    sse = 0;

    for j= 1:15

        clss =  classification(1,j);

        v = examples(1:3, j) - clss_av(:, clss);

        sse = sse + v.'*v;

    end

    %----------------------------------------
    utility = sse;



end
```

VIII Appendix B: Hardware

VIII.A Gripper

VIII.A.1 Gripper version 1.0

In order to manipulate objects and evaluate stiffness, some type of gripper needs to be mounted on top of the ATI Gamma Force sensor. The image below shows the Pro-Engineer model for a custom gripper, developed by Sam Bhattacharyya in June 2011, including an attachment to the force sensor.

This gripper is actuated by a large push style solenoid, McMaster Part# 69905K48, and the solenoid is housed within the large cylindrical portion of the gripper. The solenoid has a stroke of approximately 20mm while assembled within the gripper, and the gripper is able to grip down with a force of ~10 N.

The gripper is almost entirely manufactured out of ABS, via rapid prototyping. The associated files are available at arma.vuse.vanderbilt.edu/mediawiki

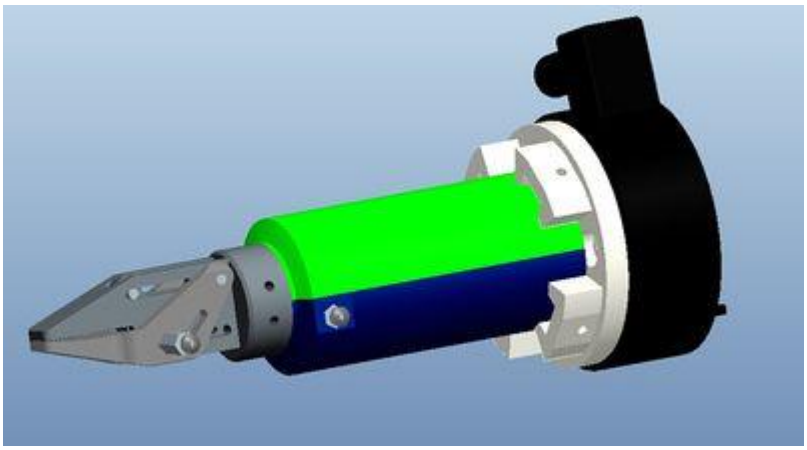

Figure A.8: Puma Gripper Pro-E model, V 1.0

Electronics setup for gripper + relay

The solenoid is a simple on/off mechanism that pushes/extends a rod outwards when a specified voltage, at high enough current, applied across the solenoid's leads (polarity doesn't actually matter). The resulting control circuit is actually quite simple, and is detailed in the image to the right.

Below is a table including the parts used in the electronic setup, which were ordered from **OnlineComponents.com**

Part number	Description
1-1393788-6	5V 5A Relay
2N3392	NPN Transistor
1.5KE100CA/54	Diode
RL020S222G	Resistor

These components were organized into the following circuit

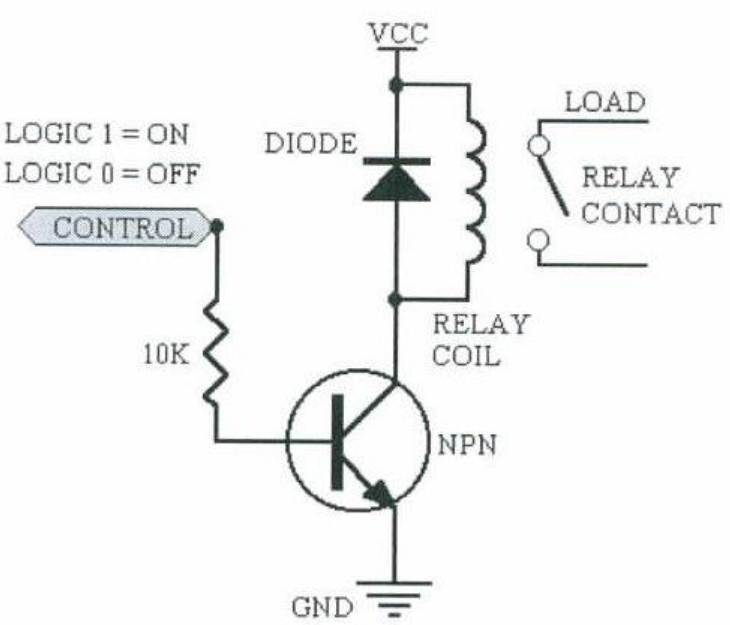

Figure A.9: Puma gripper v 1.0 relay circuit

VIII.A.2 Gripper 2.0

Design:

Due to a lack of gripping force, and limited functionality, the Puma's Gripper 1.0 was significantly redesigned. The new design uses a motor and worm-gear drive instead of a solenoid as the principle actuation mechanism. This new gripper should theoretically output a gripping force of 86 Newtons, and is much more flexible in terms of gripper-head design. This design was created by Sam Bhattacharyya on October 14, 2011, and was intended for the Global Stiffness exploration project, but designed for general purpose use.

Below is an attached Pro-Engineer image of the design. The housing was designed to be made using laser cut parts, and to be attached to the ATI-Gamma force sensor, via a custom rapid prototyped attachment.

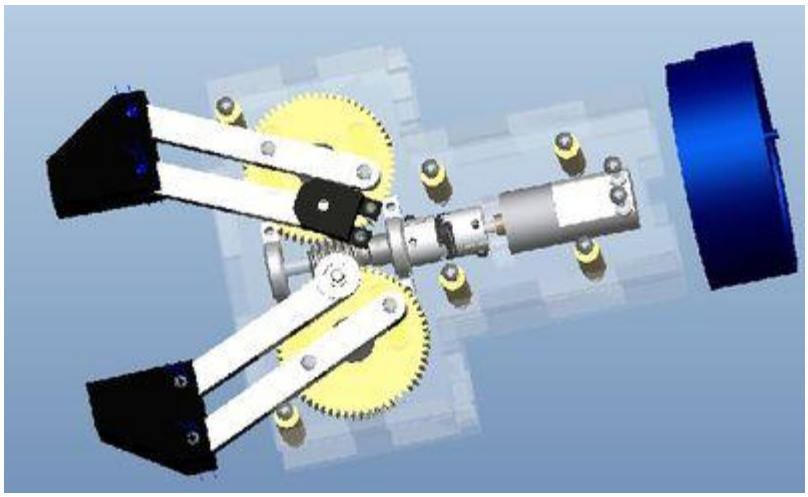

Figure A.10: Puma gripper v 2.0 Pro-Engineer model

Specifications

Overview

- Gripping Force: 86.4 N
- Actuation time: 1.375 s
- Weight: .8824 kg
- Center of Grip: 185 mm along Force sensor Z axis

Force analysis

Motor specifications for Pololu 29:1 Metal Gear Motor

- Operating Voltage: 6V
- Free run speed: 440 rpm
- Stall Current: 3.3 Amps
- Stall Torque: .18Nm

Transmission Specification (Worm drive x1)

- Gear ratio: 60:1
- Worm Gear SDP-SI Part # A 1B 6MYH08R060
    - Module: .80
    - # of Teeth: 60
    - Gear Ratio: 60:1
    - Pitch Diameter: 48.00 mm

- Worm SDP-SI Part # A 1Y 5MYK08RA
    - Module: .8
    - Pitch diameter: 10.4mm
    - Leads: 1
    - Hub Configuration: 5mm bore, with set screw

End effector Specification

- Lever arm: 75 mm
- Range of motion: 0 - 65 mm
- Angular range of motion:0 - 110 degrees (between arms), 0 - 55 degrees per arm
- Gripper force: 86.4 N
    - Force = [(Lever Arm)^-1]*[(Motor Torque)*(Gear Ratio)*(Gear Efficiency)]
    - Force = (.075 m)^-1*(.18 Nm)*(60)*(.6)
- Actuation time: 1.375 seconds
    - Angular Speed = (Motor Speed)*(Speed Efficiency @ No load)*(Gear Ratio)^-1
    - Angular Speed = 40 deg/s = 6.6 rpm = (400 rpm)*(90%)*(60)^-1
    - Actuation time = (Angular range of motion)/(Angular speed)

Weight:

The approximate weight of the gripper is .8843 kg, numerically calculated from the Pro-Engineer model. With respect to the coordinate frame of the ATI Gamma Force sensor, via the specified attachment block, the center of gravity of the Gripper is located in the table below:

Coordinate	Distance
X	0 mm
Y	-9.003mm
Z	100.005 mm

Parts list

The table below shows the list of commercial parts which were ordered for this particular project.

Parts	Quantity	Supplier	Part #	Price Each	Price Total
Acrylic of Enclosure	6	Delvie\'s Plastics	250-12x12	5	30
Potentiometer	2	Digikey	3382G-1-253GCT-ND	2.17	4.34
Drive Shaft	1	McMaster	6112K37	8.04	8.04
Spacers	7	McMaster	93295A113	0.99	6.93
Spacers	6	McMaster	93295A088	0.37	2.22
Spacer bearing gripper head	4	Mcmaster	92474A026	1.43	5.72
Gripper Head screws, 2-56	1	McMaster	91772A084	4.27	4.27
4 mm Pins	1	McMaster	93600A137	7.33	7.33
M2 x 10	1	McMaster	92005A033	3.23	3.23
Motor	1	Pololu	1163	19.99	19.99
5MM Bearing w/ pillow block	2	SDP-SI	A 7Z29MXS005	13.21	26.42
Worm	1	SDP-SI	A 1Y 5MYK08RA	26.35	26.35
Bearing	2	SDP-SI	A 7Y 5MF1304	9.23	18.46
Oldham Couping	1	SDP-SI	A 5P15M3315	2.04	2.04
Oldham clamps	2	SDP-SI	A 5A15M331504	9.01	18.02
Worm Gear	2	SDP-SI	A 1B 6MYH08R060	45.35	90.7
				Total Cost:	274.06

VIII.B Experimental Setup

VIII.B.1 Rigid triangle Experiment

The main structure of the rigid triangle experiment was created via laser cutting of ¼'' acrylic sheets of plastic.

Figure A.11: Rigid triangle fully setup, with spring

Two primary pieces were cut out of acrylic: The frame itself (below, left), and the rigid triangle (below, right).

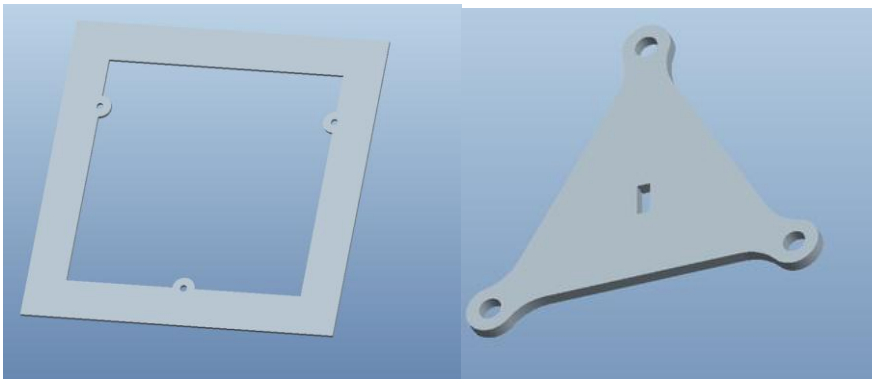

Figure A.12: The rigid triangle experiment setup-components

The length of the side of each triangle is $40mm$, the length of the laser cut frame was 1 ftx1ft, with a thickness a border thickness of 1’’.

The springs used were simple linear 1kN/m springs, McMaster Part number 9654K125. The unstreched length of each spring was 31.75mm, and there were two springs, hooked in series, between each vertex of the triangle, and it’s fixed location on the environment.